Senescent cells inhibit muscle differentiation via the SASP-lipid 15d-PGJ_2 mediated modification and control of HRas

Swarang Sachin Pundlik[1,2], Alok Barik[1], Ashwin Venkateshvaran[1], Snehasudha Subhadarshini Sahoo[1,3], Mahapatra Anshuman Jaysingh[4,5], Raviswamy G H Math[6], Arvind Ramanathan[1,*]

1. Metabolic Regulation of Cell Fate (RCF), Institute for Stem Cell Science and Regenerative Medicine (InStem), Bangalore Life Science Cluster, GKVK-Post, Bellary Road, Bengaluru, Karnataka-560065, India.
2. Manipal Academy of Higher Education (MAHE), Tiger Circle Road, Madhav Nagar, Manipal, Karnataka-576104, India.
3. University of North Carolina at Chapel Hill, 216 Lenoir Dr, Chapel Hill, North Carolina-27599 U. S. A.
4. Department of Biological Sciences, Indian Institute of Science Education and Research Kolkata (IISER-K), Campus Road, Mohanpur, West Bengal-741246, India.
5. Division of Biology and Biomedical Sciences, Washington University in St Louis, 1 Brookings Dr, St. Louis, Missouri-63130, U. S. A.
6. National Centre for Biological Sciences (NCBS), Rajiv Gandhi Nagar, Kodigehalli, Bengaluru, Karnataka-560065, India.

* All correspondence should be written to Dr. Arvind Ramanathan at arvind@instem.res.in

Abstract

Senescent cells, which are characterized by multiple features such as increased expression of Senescence-Associated β-galactosidase activity (SA β-gal) and cell cycle inhibitors such as p21 or p16, accumulate with tissue damage and dysregulate tissue homeostasis. In the context of skeletal muscle, it is known that agents used for chemotherapy such as Doxorubicin cause buildup of senescent cells, leading to the inhibition of tissue regeneration. Senescent cells influence the neighboring cells via numerous secreted factors which form the senescence-associated secreted phenotype (SASP). Lipids are emerging as a key component of SASP that can control tissue homeostasis. Arachidonic acid-derived lipids have been shown to accumulate within senescent cells, specifically 15d-PGJ_2, which is an electrophilic lipid produced by the non-enzymatic dehydration of the prostaglandin PGD_2. In this study, we show that 15d-PGJ_2 is also released by Doxorubicin-induced senescent cells as a SASP factor. Treatment of skeletal muscle myoblasts with the conditioned medium from these senescent cells inhibits myoblast fusion during differentiation. Inhibition of L-PTGDS, the enzyme that synthesizes PGD_2, diminishes the release of 15d-PGJ_2 by senescent cells and restores muscle differentiation. We further show that this lipid post-translationally modifies Cys184 of HRas in skeletal muscle cells, causing a reduction in the localization of HRas to the Golgi, increased HRas binding to RAF RBD, and activation of cellular MAPK-Erk signaling (but not the Akt signaling). Mutating C184 of HRas prevents the ability of 15d- PGJ_2 to inhibit the differentiation of muscle cells and control the activity of HRas. This work shows that 15d-PGJ_2 released from senescent cells could be targeted to restore muscle homeostasis after chemotherapy.

Introduction

Senescent cells are important drivers of aging and damage-associated loss of tissue homeostasis(Childs et al., 2015). Anti-cancer chemotherapy presents an important context where treatment with chemotherapeutics such as Doxorubicin (Doxo) causes widespread cellular senescence which inhibits tissue homeostasis and regeneration, including in skeletal muscles(Francis et al., 2022). It has been shown that Doxo causes systemic inflammation and leads to the emergence of senescent cells across tissues(Di Leonardo et al., 1994; Hu and Zhang, 2019; Robles and Adami, 1998). Senescent cells negatively affect tissue homeostasis and regeneration by releasing factors including proteins like growth factors, matrix metalloproteases, cytokines, and chemokines, and small molecules like fatty acid derivatives(Campisi, 2005; Coppé et al., 2010; Dilley et al., 2003; Krtolica et al., 2001; Parrinello et al., 2005; Shelton et al., 1999; Yang et al., 2006). The release of these factors from senescent cells is called the Senescence-Associated Secretory Phenotype (SASP). It is expected that these SASP factors and their mechanisms of action will vary depending on cellular and tissue contexts. Identifying SASP factors and their underlying mechanistic targets will be critical for building an understanding of how senescent cells control tissue homeostasis(Coppé et al., 2010; Davalos et al., 2010). Lipids are a less explored family of SASP factors, and it is important to understand how they affect tissue regeneration(Hamsanathan and Gurkar, 2022). We have previously shown that senescent cells have increased intracellular levels of prostaglandin 15d-PGJ_2(Wiley et al., 2021), a non-enzymatic dehydration product of prostaglandin PGD_2(Shibata et al., 2002). In the context of skeletal muscle, PGD_2 and 15d-PGJ_2 have been shown to negatively regulate muscle differentiation via mechanisms that do not depend on a cognate receptor(Hunter et al., 2001; Veliça et al., 2010). Here we study the role of 15d-PGJ_2 as a member of the SASP and identify the mechanisms by which it might negatively affect muscle regeneration. 15d-PGJ_2 has been previously shown to covalently modify multiple proteins like MAPK1, MCM4, EIF4A-I, PKM1, GFAP etc. in endothelial and neuronal cells(Marcone and Fitzgerald, 2013; Yamamoto et al., 2011). 15d-PGJ_2 was shown to be covalently modifying HRas in NIH3T3, Cos1, and IMR90 cell lines(Luis Oliva et al., 2003; Wiley et al., 2021). We further studied HRas as an important target that might mediate the effects of 15d-PGJ_2 on muscle differentiation via covalent modification. We investigated HRas as a possible effector of 15d-PGJ_2

because (i) HRas belongs to the Ras superfamily of small molecule GTPases and is a known regulator of key cellular processes(Davis et al., 1983; Harvey, 1964; Kirsten and Mayer, 1967; Vetter and Wittinghofer, 2001). (ii) constitutively active HRas mutant (HRas V12) has been shown to inhibit the differentiation of myoblasts by inhibiting MyoD and Myogenin expression(Konieczny et al., 1989; Lassar et al., 1989; Olson,' et al., 1987; Van Der Burgt et al., 2007). (iii) Downstream signaling of HRas is important for muscle homeostasis as skeletal and cardiac myopathies are observed in individuals carrying constitutively active mutants of HRas(Engler et al., 2021; Konieczny et al., 1989; Lee et al., 2010; Olson,' et al., 1987; Scholz et al., 2009; Van Der Burgt et al., 2007). HRas is highly regulated by lipid modifications, it undergoes reversible palmitoylation and de-palmitoylation at C-terminal cysteines, which regulate the intracellular distribution and activity of HRas(Gutierrez et al., 1989; Lu and Hofmann, 1995; Rocks et al., 2005). In this study, we show that 15d-PGJ_2 is synthesized and released by senescent myoblasts upon treatment with Doxo. 15d-PGJ_2, taken up by the myoblasts, covalently modifies HRas at cysteine 184 and activates it. We also show that previously reported inhibition of differentiation of myoblasts by 15d-PGJ_2 depends on HRas C-terminal cysteines, notably cysteine 184. This study provides a mechanism by which prostaglandins secreted as SASP inhibit the differentiation of myoblasts, affecting muscle homeostasis in patients undergoing chemotherapy.

Results

Doxorubicin (Doxo) treatment induces senescence in mouse skeletal muscles and C2C12 mouse myoblasts.

Doxorubicin-mediated DNA damage has been shown to induce senescence in cells(Di Leonardo et al., 1994; Hu and Zhang, 2019; Robles and Adami, 1998). Therefore, we injected B6J mice intraperitoneally with Doxorubicin (Doxo) (5mg/kg) every 3 days for 9 days and observed induction of DNA damage-mediated senescence in hindlimb skeletal muscles (Fig. S1A). We observed an increase in the expression of p21 and increased nuclear levels of the DNA damage marker γH2A.X in mouse Gastrocnemius muscles (Fig. 1A and B). We also observed a significant increase in the mRNA levels of known senescence markers (p16 and p21), SASP factors (CXCL1, CXCL2, TNF1α, IL6, TGFβ1) in skeletal muscles of mice treated with Doxo compared to that of mice

treated with saline (Fig. 1C). These observations suggest that there is induction of senescence in skeletal muscles of mice upon treatment with Doxo.

C2C12 cells have been shown to undergo senescence after DNA damage, as assessed by an increase in the levels of SA β-gal and known markers of SASP (IL1α, IL6, CCL2, CXCL2, CXCL10)(Moiseeva et al., 2022). We treated C2C12 myoblasts with Doxo (150 nM) and observed a significant increase in the size of the nuclei (Fig. 1D), flattened cell morphology with an increase in the cell size (Fig. 1E), a significant increase in the mRNA levels of cell cycle inhibitor p21 and SASP factors IL6 and TGFβ (Fig. 1F), a significant increase in the protein levels of p21 (Fig. 1G), and an increase in the levels of SA β-gal (Fig. 1H) in C2C12 cells treated with Doxo. These observations suggest that C2C12 cells undergo senescence upon treatment with Doxo.

Doxo-mediated senescence induces synthesis and release of 15d-PGJ_2 in C2C12 myoblasts and mouse skeletal muscle.

Synthesis of prostaglandins by senescent cells has previously been reported(Wiley et al., 2021; Wiley and Campisi, 2021). Specifically, levels of PGD_2 and its metabolite 15d-PGJ_2 have been shown to be significantly increased in senescent cells. Therefore, we measured the levels of mRNA of enzymes involved in the synthesis of PGD_2/15d-PGJ_2 (PTGS1, PTGS2, and PTGDS), in the gastrocnemius muscle of mice after treatment with Doxo. We observed a significant increase in the mRNA levels of PTGS1, PTGS2, and PTGDS enzymes in the skeletal muscle of mice treated with Doxo (Fig. 1C). We also observed a time-dependent increase in the mRNA levels of PTGS1, PTGS2, PTGDS, and PTGES enzymes in C2C12 cells treated with Doxo compared to Day 0 (Fig. 1I). Expression of enzyme PTGES was elevated on Day 4, whereas the expression of Prostaglandin D synthase (PTGDS) increased only after Day 8, reaching maximum expression on Day 12. These observations suggest an increase in the synthesis of prostaglandins in senescent cells.

15d-PGJ_2 is a non-enzymatic dehydration product of PGD_2(Shibata et al., 2002). We observed an increase in the mRNA levels of synthetic enzymes of 15d-PGJ_2 in senescent C2C12 cells. Therefore, we measured the levels of 15d-PGJ_2 released by senescent C2C12 cells using targeted mass spectrometry (Fig. S1C, D, E, and F). The concentration of 15d-PGJ_2 was quantified by monitoring the transition of the m/z of

ions from 315.100 ➔ 271.100 using a SCIEX 6500 mass spectrometer. We plotted a standard curve using purified 15d-PGJ_2 (Fig. S1F) to quantify the concentration of 15d-PGJ_2. We used the representative peaks from the conditioned medium collected from C2C12 cells incubated in 0.2% serum medium for 3 days (Quiescent cells) and C2C12 cells treated with Doxo (150 nM) (Senescent cells) to measure the concentration of 15d-PGJ_2 released by quiescent cells or senescent C2C12 cells. We observed a significant increase (~100 fold) in the concentration of 15d-PGJ_2 in the conditioned medium from senescent cells as compared to that in quiescent cells (Fig. 1J). This suggests that senescent C2C12 cells release 15d-PGJ_2 in the medium.

Prostaglandin PGD_2 and its metabolites in the conditioned medium of senescent cells inhibit the differentiation of C2C12 myoblasts.

15d-PGJ_2 (the final non-enzymatic dehydration product of PGD_2) has been shown to inhibit the differentiation of myoblasts(Hunter et al., 2001). We observed the release of 15d-PGJ_2 by senescent cells, showing that 15d-PGJ_2 is a SASP factor (Fig. 1F). Conditioned medium of senescent cells inhibits the differentiation of myoblasts in myotonic dystrophy type 1(Conte et al., 2023). Therefore, we tested whether 15d-PGJ_2, the terminal dehydration product of PGD_2, is required for the inhibitory effect of SASP on the differentiation of myoblasts. We treated C2C12 myoblasts with the conditioned medium of senescent cells or senescent cells treated with 30 μM of AT-56 (a well-characterized inhibitor of prostaglandin D synthase (PTGDS))(Hu et al., 2021; S. Hu et al., 2023; Shunfeng Hu et al., 2023; Irikura et al., 2009) and measured the differentiation of myoblasts by calculating the fusion index. We observed a significant decrease (~20%) in the fusion index of the C2C12 myoblasts treated with the conditioned medium of senescent cells (Fig. 2A), suggesting that SASP factors decrease the differentiation of myoblasts. This decrease in the inhibition was rescued in myoblasts treated with the conditioned medium of senescent cells treated with AT-56 (Fig. 2A). This suggests that prostaglandins PGD_2/15d-PGJ_2 released by senescent cells as SASP factors can inhibit the differentiation of myoblasts.

15d-PGJ_2 inhibits the proliferation and differentiation of mouse and human myoblasts.

15d-PGJ_2 has been shown to affect the proliferation of cancer cell lines, both positively and negatively (Chen et al., 2003; Choi et al., 2020; Slanovc et al., 2024; Yen et al.,

2014). We measured the effect of 15d-PGJ_2 on the proliferation of C2C12 myoblasts. We treated C2C12 myoblasts with 15d-PGJ_2 (10 μM) or DMSO in DMEM 10% Serum medium for 72 hours and observed a significant decrease in the proliferation of C2C12 cells after treatment with 15d-PGJ_2 (Fig. 2B). The doubling time of C2C12 cells was also increased upon treatment with 15d-PGJ_2 (57.24 hours) compared to DMSO (13.76 hours). This suggests that 15d-PGJ_2 decreases the proliferation of C2C12 myoblasts.

We measured the differentiation of C2C12 mouse and primary human myoblasts after treatment with 15d-PGJ_2. To rule out the toxic effects of 15d-PGJ_2 on cell physiology, we treated C2C12 cells with 15d-PGJ_2 (1 μM, 2 μM, 4 μM, 5 μM, and 10 μM) in the C2C12 differentiation medium, and measured the viability of cells after 24 hours of treatment, using an MTT viability assay. We judged that 15d-PGJ_2 was not cytotoxic up to 5 μM in the C2C12 differentiation medium (Fig. S2A). Based on this, we treated differentiating myoblasts with 15d-PGJ_2 (1 μM, 2 μM, and 4 μM) for 5 days to measure the effects of 15d-PGJ_2 treatment on differentiation of myoblasts. We observed a dose-dependent decrease in the mRNA levels of MyoD, MyoG, and MHC in differentiating C2C12 cells after treatment with 15dPGJ_2 (Fig. 2C). There was a significant decrease in the no. of nuclei in individual MHC^{+ve} fiber (~75%) in C2C12 cells treated with 15d-PGJ_2 (4 μM) compared to DMSO (Fig. 2D), suggesting a decrease in the fusion of myoblasts in myotubes. We also observed a dose-dependent decrease in the protein levels of MHC in differentiating primary human myoblasts upon treatment with 15d-PGJ_2 (Fig. 2E). Together, these observations suggest that 15d-PGJ_2 inhibits the differentiation of both mouse and human myoblasts.

Biotinylated 15d-PGJ_2 covalently modifies HRas at Cysteine 184.

15d-PGJ_2 has been shown to covalently modify several proteins including p53 and NF-κB, which are involved in several key biological processes(Marcone and Fitzgerald, 2013). HRas was identified to be covalently modified by 15d-PGJ_2 at cysteine 184 in NIH3T3 and Cos1 cells(Luis Oliva et al., 2003). Therefore, we tested whether 15d-PGJ_2 could covalently modify HRas in C2C12 cells. We treated C2C12 cells expressing the EGFP-tagged wild-type HRas with biotinylated 15d-PGJ_2 (5 μM). We then immunoprecipitated biotinylated 15d-PGJ_2 using streptavidin. We observed a significant increase (~3.5 fold) in the pulldown of HRas upon treatment with 15d-PGJ_2-

biotin compared to DMSO (Fig. 3A), suggesting an interaction between 15d-PGJ_2 and HRas. To measure the role of individual C-terminal cysteines in the binding of HRas with 15d-PGJ_2, we treated C2C12 cells expressing the EGFP-tagged C181S and C184S mutants of HRas with biotinylated 15d-PGJ_2 (5 μM), and immunoprecipitated using streptavidin. We observed that the intensity of EGFP-tagged HRas was significantly decreased in cells expressing the C184S mutant (~80% decrease compared to HRas WT) but not in those expressing the C181S mutant (Fig. 3A). This suggests that 15d-PGJ_2 covalently modifies HRas at cysteine 184 in C2C12 cells.

15d-PGJ_2 increases the FRET between EGFP-HRas and mCherry-RAF-RBD in wild-type and C181S mutant but not in the C184S mutant of HRas.

We next tested the effect of covalent modification of HRas by 15d-PGJ_2 on HRas GTPase activity using FRET. mCherry-RAF-RBD is a well-characterized sensor of the activity of HRas. RAF-RBD binds to the activated HRas upon activation of HRas, allowing FRET between EGFP and mCherry(Rocks et al., 2005). We co-expressed EGFP-tagged HRas (EGFP-HRas) with mCherry-RAF-RBD in C2C12 myoblasts (Fig. 3B). We measured the efficiency of FRET between EGFP and mCherry using an ImageJ plugin, FRET analyzer(Hachet-Haas et al., 2006). We compared the mean acceptor normalized FRET index in C2C12 myoblasts co-expressing EGFP-HRas WT and mCherry-RAF-RBD before and after treatment of 15d-PGJ_2 (10 μM) for 1 hour. We observed a significant increase (~30%) in the mean acceptor normalized FRET index upon treatment with 15d-PGJ_2 (Fig. 3C). This suggests that 15d-PGJ_2 activates HRas. To measure the role of individual C-terminal cysteines in 15d-PGJ_2 mediated activation of HRas, we co-expressed EGFP-HRas C181S or C184S with mCherry-RAF-RBD in C2C12 myoblasts. We measured the mean acceptor normalized FRET index before and after 1 hour of treatment with 15d-PGJ_2 (10 μM). We observed a significant increase (~40%) in the mean acceptor normalized FRET index in cells expressing EGFP-HRas C181S upon treatment with 15d-PGJ_2 but not in cells expressing EGFP-HRas C184S (Fig. 3D). These observations suggest that activation of HRas by 15d-PGJ_2 occurs in a cysteine 184 dependent manner.

15d-PGJ_2 increases phosphorylation of Erk (Thr202/Tyr204) but not Akt (S473) in C2C12 myoblasts.

HRas regulates two major downstream signaling pathways, the MAP kinase (MAPK) pathway and the PI3 kinase (PI3K) pathway(Pylayeva-Gupta et al., 2011). We tested the effects of treatment with 15d-PGJ_2 on these two downstream signaling pathways by measuring the phosphorylation of Erk (42 kDa and 44 kDa) and Akt proteins in C2C12 cells. We treated C2C12 cells with 15d-PGJ_2 (5 μM and 10 μM) or DMSO for 1 hr (after 24 hrs. of serum starvation) and observed a dose-dependent increase in the phosphorylation of Erk (T202/Y204) (42 kDa) but not of Erk (44 kDa) (Fig. 3E). We did not observe an increase in the phosphorylation of Akt (S473) in C2C12 cells after treatment with 15d-PGJ_2 (Fig. S3C). These observations suggest that 15d-PGJ_2 activates the MAPK signaling pathway, but not the PI3K signaling pathway.

15d-PGJ_2 contains a reactive electrophilic center in its cyclopentenone ring, that can react with cysteine residues of proteins(Luis Oliva et al., 2003). We tested its role in activating the MAPK signaling pathway. We measured the phosphorylation of Erk (42kDa and 44 kDa) in C2C12 cells after treatment with cells with 9,10-dihydro-15d-PGJ_2 (10 μM), a 15d-PGJ_2 analog which is devoid of the electrophilic center, for 1 hr (after 24 hr. of serum starvation). We observed that the phosphorylation of Erk (42 kDa and 44 kDa) in C2C12 cells treated with 9,10-dihydro-15d-PGJ_2 was significantly reduced (~70%) as compared to the treatment with 15d-PGJ_2 (Fig. 3F). This shows that 15d-PGJ_2 activates the HRas-MAPK signaling pathway via the electrophilic center in its cyclopentenone ring.

15d-PGJ_2 increases the localization of EGFP-tagged HRas at the plasma membrane compared to the Golgi in a C-terminal cysteine-dependent manner.

15d-PGJ_2 covalently modifies cysteine 184 and activates HRas signaling (Fig. 3). Reversible palmitoylation of cysteine 181 and cysteine 184 in the C-terminal tail of HRas regulate intracellular distribution and signaling of HRas. Inhibition of palmitoylation of the C-terminal cysteine 181, either by a palmitoylation inhibitor 2-Bromopalmitate or by mutation to serine, causes accumulation of HRas at the Golgi compared to the plasma membrane and alters activity(Rocks et al., 2005). Therefore, we tested whether the modification of 15d-PGJ_2 alters the intracellular distribution of HRas. We co-expressed the EGFP-tagged wild type and the cysteine mutants of HRas (EGFP-HRas WT/C181S/C184S) with a previously reported marker of Golgi(Shaner et al., 2008) in C2C12 cells and stained the cells with plasma membrane marker WGA-

633 (Fig. 4A). We compared R_{mean}, the ratio of mean EGFP-HRas intensity at the Golgi to the mean HRas intensity at the plasma membrane, to measure the distribution of HRas between the plasma membrane and the Golgi. We measured the intracellular distribution of HRas between the Golgi and the plasma membrane in C2C12 cells after treatment with 15d-PGJ_2 (10 μM) for 24 hours in DMEM 10% serum medium and observed a significant decrease (~20%) in the R_{mean} of C2C12 cells expressing the wild-type HRas after treatment with 15d-PGJ_2 (Fig. 4B). However, we did not observe a change in the R_{mean} of C2C12 cells expressing HRas C181S or HRas C184S after treatment with 15d-PGJ_2 (Fig. 4C). These observations suggest that 15d-PGJ_2 increases the localization of HRas at the plasma membrane as compared to that in the Golgi in an HRas C-terminal cysteine-dependent manner.

15d-PGJ_2 mediated inhibition of differentiation of C2C12 cells is rescued by C181S and C184S mutants of HRas.

HRas inhibits the differentiation of C2C12 myoblasts(Engler et al., 2021; Konieczny et al., 1989; Lassar et al., 1989; Lee et al., 2010; Olson,' et al., 1987; Scholz et al., 2009; Van Der Burgt et al., 2007).15d-PGJ_2 covalently modifies cysteine 184 and activates HRas (Fig. 3). Therefore, we tested whether the inhibition of myoblast differentiation by 15d-PGJ_2 depends on the activation of HRas signaling by modification of the C-terminal cysteine 184. We expressed the wild-type and the cysteine mutants of HRas (EGFP-HRas WT/C181S/C184S) in C2C12 myoblasts and treated the cells with 15d-PGJ_2 (4 μM) or DMSO during differentiation. We observed a decrease in the levels of mRNA of MHC in C2C12 cells expressing HRas WT and HRas C181S after 5 days of treatment with 15d-PGJ_2. We did not observe this in expressing HRas C184S (Fig. 4D). We also observed a significant decrease in the protein levels of MHC in differentiating C2C12 cells expressing HRas WT and HRas C181S after treatment with 15d-PGJ_2 (Fig. 4E). This decrease was partially rescued in cells expressing HRas C184S (Fig. 4E). These observations suggest that the inhibition of myoblast differentiation by 15d-PGJ_2 depends on modification of HRas C-terminal cysteine 184.

Discussion

Senescence is characterized by an irreversible arrest in cell proliferation(Hayflick, 1965). Cells undergo senescence because of a myriad of stresses, including DNA damage, mitochondrial damage, and oncogene overexpression(Bihani et al., 2007,

2004; Casar et al., 2018; Chen and Ames, 1994; Chen et al., 1998; Coppé et al., 2008; D'Adda Di Fagagna, 2008; D'Adda Di Fagagna et al., 2003; Di Leonardo et al., 1994; Franza et al., 1986; Land et al., 1983; Robles and Adami, 1998; Serrano et al., 1997; Wiley et al., 2016; Woods et al., 1997). Senescent cells exhibit a multi-faceted physiological response, where they exhibit a flattened morphology, increase in cell size(Chen and Ames, 1994; Serrano et al., 1997), upregulation of tumor suppressor proteins(Calabrese et al., 2009; Lowe et al., 2004; Stein et al., 1990; Zindy et al., 2003), expression of neutral pH active β-galactosidase (SA β-gal)(Dimri et al., 1995; Lee et al., 2006), and altered metabolic state(Bittles and Harper, 1984; Jones et al., 2005; Wiley and Campisi, 2021, 2016; Zwerschke et al., 2003). Arachidonic acid metabolism is upregulated in senescent cells, which leads to increased synthesis of eicosanoid prostaglandins, which regulate the physiology of senescent cells(Wiley et al., 2021; Wiley and Campisi, 2021). Senescent cells exhibit a secretory phenotype (SASP) consisting of a variety of bioactive molecules including cytokines and chemokines, growth factors, matrix metalloproteases, etc(Coppé et al., 2008). Senescent cells influence the surrounding cells via the SASP factors, which regulate proliferation, migration, and other cell biological processes in the neighboring cells(Campisi, 2005). SASP-mediated perturbations in the microenvironment are implicated in several senescence-associate pathologies(Wiley and Campisi, 2021). Senescent fibroblasts increase the proliferation of premalignant and malignant epithelial cells(Krtolica et al., 2001). Conditioned medium of senescent fibroblasts promoted tumorigenesis in mouse keratinocytes(Dilley et al., 2003). Senescent fibroblasts transform pre-malignant breast cancer cells into invasive, tumor-forming cells(Parrinello et al., 2005). Senescence in muscle stem cells induces sarcopenia via activation of the p38 MAP kinase pathway and transient inhibition of the p38 MAP kinases rejuvenates aged muscle stem cells to ameliorate sarcopenia(Cosgrove et al., 2014). Senescent cells inhibit the differentiation of myoblasts by secretion of IL6 by senescent muscle stem cells in myotonic dystrophy(Conte et al., 2023).

In this study, we show that senescent myoblasts synthesize and release eicosanoid prostaglandin 15-deoxy-$\Delta^{12,14}$-prostaglandin J_2 (15d-PGJ_2) (Fig. 1I and J), the terminal non-enzymatic dehydration product of prostaglandin PGD_2(Shibata et al., 2002). We used Doxorubicin (Doxo) to induce senescence in C2C12 myoblasts and showed that the conditioned medium of senescent C2C12 cells inhibits differentiation of C2C12

myoblasts (Fig. 2A). Inhibition of synthesis of PGD_2 by treatment of senescent cells with AT-56, a well-characterized inhibitor of prostaglandin D synthase(Hu et al., 2021; S. Hu et al., 2023; Shunfeng Hu et al., 2023; Irikura et al., 2009), rescued this inhibitory effect of the conditioned medium on the differentiation of myoblasts (Fig. 2A). A study has shown that prostaglandin PGD_2 inhibits differentiation of C2C12 myoblasts(Veliça et al., 2010), but the authors noted that knockout of DP1 and DP2 (the known receptors of prostaglandins PGD_2) does not abrogate inhibition of differentiation of myoblasts by PGD_2. This observation suggested that PGD_2 might inhibit the differentiation of myoblasts by a receptor-independent mechanism, possibly by its spontaneous non-enzymatic dehydration to 15d-PGJ_2. 15d-PGJ_2 has been suggested to be an endogenous ligand of PPARγ(Li et al., 2019). However, the inhibition of PPARγ did not abrogate the inhibition of differentiation of C2C12 myoblasts by 15d-PGJ_2, suggesting the existence of other possible mechanisms(Hunter et al., 2001). 15d-PGJ_2 has varied effects on cell physiology in a context-dependent manner. On one hand, 15d-PGJ_2 promotes tumorigenesis by inducing epithelial to mesenchymal transition in breast cancer cell line MCF7(Choi et al., 2020), 15d-PGJ_2 inhibits the proliferation of A549, H1299, and H23 lung adenocarcinoma cells via induction of ROS and activation of apoptosis(Slanovc et al., 2024). Here, we show that 15d-PGJ_2 inhibits the proliferation and the differentiation of C2C12 myoblasts (Fig. 2B, C and D).

15d-PGJ_2 contains an electrophilic cyclopentenone ring in its structure, allowing 15d-PGJ_2 to covalently modify and form Michael adducts with cysteine residues of proteins(Shibata et al., 2002). A previous proteomic study in endothelial cells showed biotinylated 15d-PGJ_2 covalently modified over 300 proteins, which regulate several physiological processes including cell cycle (MAPK1, MCM4), cell metabolism (Fatty acid synthase, Isocitrate dehydrogenase), apoptosis (PDCD6I), translation (Elongation factor 1 and 2, EIF4A-I), intracellular transport (Importin subunit β1, Exportin 2, Kinesin 1 heavy chain)(Marcone and Fitzgerald, 2013). Another proteomic study in neuronal cells suggested that 15d-PGJ_2 modifies several proteins including chaperone HSP8A, glycolytic proteins Enolase 1 and 2, GAPDH, PKM1, cytoskeleton proteins Tubulin β2b, β actin, GFAP, etc(Yamamoto et al., 2011). This study also showed modification of peptide fragments homologous to IκB kinase β, Thioredoxin, and a small molecule GTPase HRas. 15d-PGJ_2 has been shown to covalently modify HRas in NIH3T3 and Cos1 cells(Luis Oliva et al., 2003) and IMR90 cells(Wiley et al.,

2021). Modification by 15d-PGJ_2 led to the activation of HRas, judged by an increase in GTP-bound HRas. It is clear that 15d-PGJ_2 is capable of modifying numerous proteins in different contexts. Despite these observations, the functional relevance of these modifications in numerous contexts remains to be mapped. Here we focused on the role of 15d-PGJ_2 in the context of senescence and skeletal muscle differentiation. In this study, we showed that 15d-PGJ_2 covalently modifies HRas at cysteine 184 but not cysteine 181 in C2C12 myoblasts (Fig. 3A). We showed by FRET microscopy that modification of HRas by 15d-PGJ_2 in HRas WT and HRas C181S activates HRas in C2C12 cells, but 15d-PGJ_2 is unable to activate HRas C184S in this context (Fig. 3B, C, and D and Fig. S3A and B). This observation shows a direct link between the modification of HRas by 15d-PGJ_2 and the activation of HRas GTPase.

HRas activates two major downstream signaling pathways, the HRas-MAPK and the HRas-PI3K pathway(Pylayeva-Gupta et al., 2011). We showed that covalent modification of HRas by 15d-PGJ_2 via the electrophilic cyclopentenone ring activates HRas (Fig. 3C and D) and activates the HRas-MAPK pathway, demonstrated by an increase in the phosphorylation of Erk after treatment with 15d-PGJ_2 (Fig. 3E and F). However, we did not observe activation of the HRas-PI3K pathway, as we did not see an increase in the phosphorylation of Akt after treatment with 15d-PGJ_2 (Fig. S3C). MAPK and PI3K pathways are known regulators of muscle differentiation(Bennett and Tonks, 1997; Rommel et al., 1999), where inhibition of the RAF-MEK-Erk pathway or activation of the PI3K pathway promotes the differentiation of myoblasts. Preferential activation of the HRas-MAPK pathway over the HRas-PI3K pathway after treatment with 15d-PGJ_2 can be a possible mechanism by which 15d-PGJ_2 can inhibit the differentiation of myoblasts. HRas is known to regulate the differentiation of myoblasts in different contexts. Constitutively active HRas signaling by expression of oncogenic HRas mutant (HRas V12) leads to inhibition of differentiation of myoblasts(Konieczny et al., 1989; Lassar et al., 1989; Olson,' et al., 1987; Van Der Burgt et al., 2007). Here we showed that the inhibition of differentiation of myoblasts after 15d-PGJ_2 is partially rescued in cells expressing the C184S mutant of HRas but not the wild type or the C181S mutant (Fig. 4D and E and S4E). HRas C184S did not get modified by 15d-PGJ_2 (Fig. 3A). These observations suggest that the inhibition of differentiation of myoblasts by 15d-PGJ_2 is partially dependent on the covalent modification of HRas by 15d-PGJ_2.

Cysteine 181 and 184 in the C-terminal of HRas regulate the intracellular distribution of HRas between the plasma membrane and the Golgi by reversible palmitoylation and de-palmitoylation(Rocks et al., 2005). Inhibition of the palmitoylation of C-terminal cysteine 181, either by treatment with protein palmitoylation inhibitor 2-bromopalmitate or mutation of cysteine to serine, leads to accumulation of HRas at the Golgi. Intracellular localization of HRas maintains two distinct pools of HRas activity, where the plasma membrane pool shows a faster activation followed by short kinetics and the Golgi pool shows a slower activation but a sustained activation(Agudo-Ibáñez et al., 2015; Busquets-Hernández and Triola, 2021; Lorentzen et al., 2010; Rocks et al., 2005). We showed that the covalent modification of HRas by 15d-PGJ_2 alters the intracellular distribution of HRas. We showed that the covalent modification of HRas by 15d-PGJ_2 leads to an increase in the localization of the wild-type HRas at the plasma membrane compared to the Golgi (Fig. 4B). We did not observe any changes in the intracellular distribution of HRas C181S or HRas C184S after treatment with 15d-PGJ_2 (Fig. 4C). HRas C184S is not modified by 15d-PGJ_2, but HRas C181S is modified by 15d-PGJ_2 (Fig. 3A). This suggests that the intracellular redistribution of HRas due to covalent modification by 15d-PGJ_2 at cysteine 184 requires palmitoylation of cysteine 181.

Previous reports suggest that downstream signaling of HRas depends on the intracellular localization of HRas(Rocks et al., 2005; Santra et al., 2019). For example, targeted localization of HRas at the ER membrane induced expression of cell-migration genes. Localization of HRas at the plasma membrane showed a strong correlation with the expression of cell cycle genes, particularly the MAPK signaling pathway. Localization of HRas at the plasma membrane also showed a negative correlation with genes associated with the PI3K-Akt pathway. Here we showed that the intracellular distribution of HRas regulates differentiation of myoblasts. In order to show this, we used the constitutively active mutant of HRas (HRas V12) which has been shown to inhibit the differentiation of myoblasts(Engler et al., 2021; Konieczny et al., 1989; Lassar et al., 1989; Olson,' et al., 1987; Scholz et al., 2009; Van Der Burgt et al., 2007). We expressed cysteine mutants of HRas V12 in C2C12 myoblasts and found that HRas V12 C181S localized predominantly at the Golgi whereas HRas V12 and HRas V12 C184S localized at both the plasma membrane and the Golgi (Fig. S4A). When differentiated, we observed that C2C12 cells expressing HRas V12

C181S differentiated but HRas V12 or HRas V12 C184S did not differentiate (Fig. S4B, C, and D). These observations suggest alteration of intracellular distribution of HRas affects the HRas-mediated inhibition of the differentiation of myoblasts.

Doxorubicin (Doxo) is a widely used chemotherapy agent for the treatment of cancers(Johnson-Arbor and Dubey, 2022). Treatment with Doxo induces senescence. Doxo-mediated DNA damage leads to p53, p16, and p21-dependent senescence in human fibroblasts(Di Leonardo et al., 1994; Robles and Adami, 1998). On the other hand, treatment with doxorubicin leads to a decrease in muscle mass and cross-sectional area, leading to chemotherapy-induced cachexia(Hiensch et al., 2020). Several mechanisms have been proposed behind chemotherapy-induced cachexia, including the generation of reactive oxygen species(Gilliam and St. Clair, 2011), activation of proteases like calpain and caspases(Gilliam et al., 2012; Smuder et al., 2011), and impaired insulin signaling(de Lima Junior et al., 2016). This study provides a possible mechanism behind chemotherapy-induced loss of muscle mass and functioning. Induction of senescence in myoblasts by treatment with Doxo could lead to increased synthesis and release of 15d-PGJ_2 by senescent cells which could be taken up by myoblasts in the microenvironment. The lipid could covalently modify and activate HRas at cysteine 184 to inhibit the differentiation of myoblasts. Therefore, targeting the synthesis and release of 15d-PGJ_2 by senescent cells could serve as an important target to promote skeletal muscle homeostasis in cancer patients.

Figures

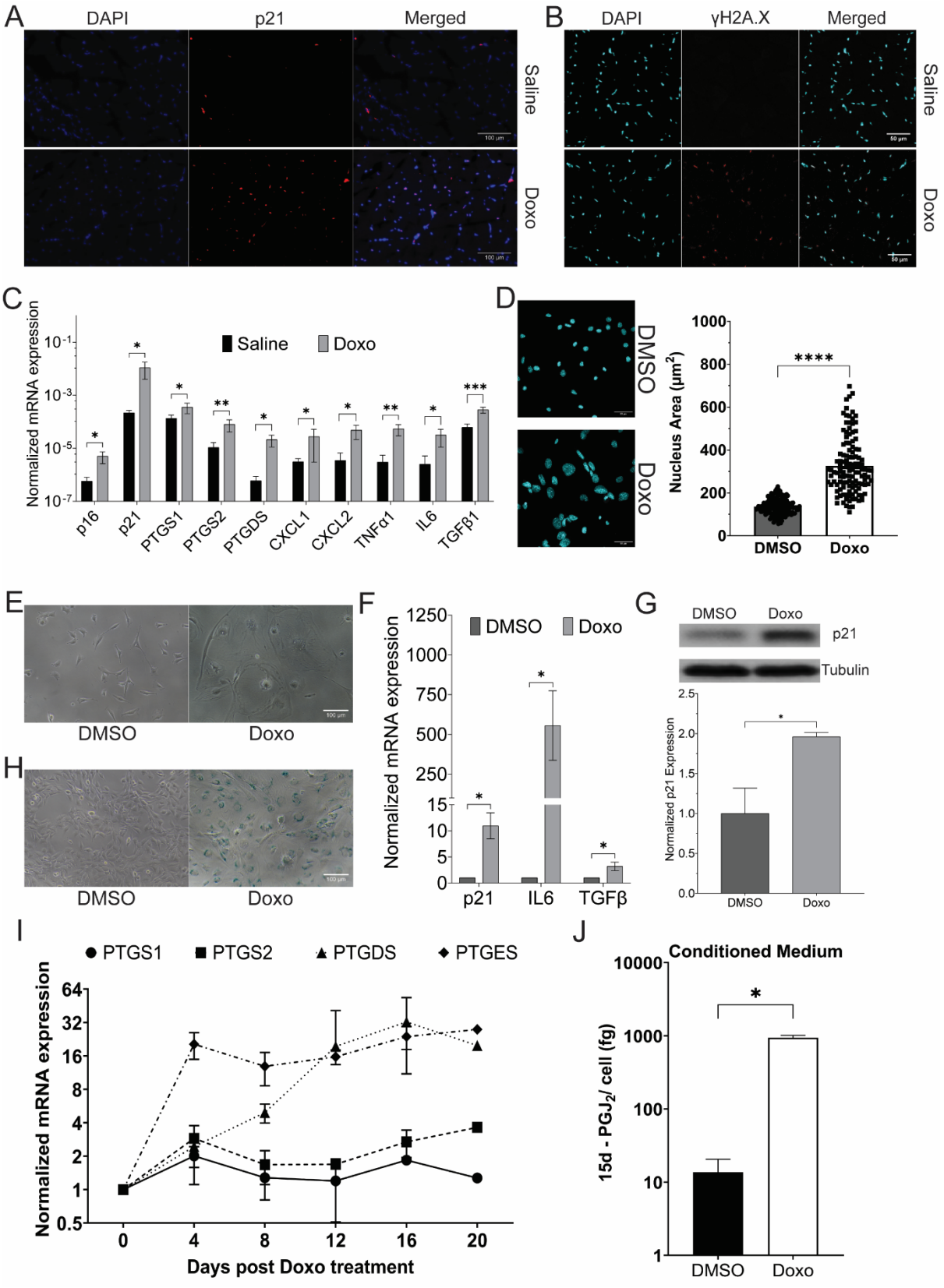

Figure 1. Prostaglandin synthesis and release by Doxo-induced senescent cells inhibits myoblast differentiation.

A. Expression and localization of tumor suppressor protein p21, measured by immunofluorescence, in hindlimb skeletal muscles of mice after 11 days of treatment with Doxo (5 mg/kg) or Saline.
B. Representative confocal micrograph of expression of γH2A.X in the gastrocnemius muscle of mice treated with Doxo (5 mg/kg) or Saline.
C. Expression of mRNAs of senescence markers (p16 and p21), SASP factors (CXCL1, CXCL2, TNFα1, IL6, TGFβ1), and enzymes involved in the biosynthesis of prostaglandin PGD_2/15d-PGJ_2 (PTGS1, PTGS2, PTGDS), measured by qPCR, in hindlimb skeletal muscles of mice after 11 days of treatment with Doxo (5 mg/kg) or Saline.
D. A representative confocal micrograph and a scatter plot of the nuclear area of C2C12 myoblasts, measured by immunofluorescence, after 16 days of treatment with Doxo (150 nM) or DMSO.
E. A representative widefield micrograph of cell morphology in C2C12 myoblasts after 16 days of treatment with Doxo (150 nM) or DMSO.
F. Expression of mRNA of cell cycle inhibitor p21 and SASP factors (IL6 and TGFβ), measured by qPCR, in C2C12 myoblasts after 16 days of treatment with Doxo (150 nM) or DMSO.
G. Expression of cell cycle inhibitor p21, measured by immunoblot, in C2C12 myoblasts after 16 days of treatment with Doxo (150 nM) or DMSO.
H. Activity of Senescence Associated β-galactosidase (SA β-gal), measured by X-gal staining at pH~6, in C2C12 myoblasts after 16 days of treatment with Doxo (150 nM) or DMSO.
I. Expression of mRNAs of prostaglandin biosynthetic enzymes, measured by qPCR, in C2C12 myoblasts after treatment with Doxo (150 nM) or DMSO.
J. Concentration of 15d-PGJ_2 released from quiescent or senescent C2C12 cells.

(Statistical significance was tested by the two-tailed student's t-test ns=$p>0.05$, *=$p<0.05$, **=$p<0.01$, ***=$p<0.001$, ****=$p<0.0001$)

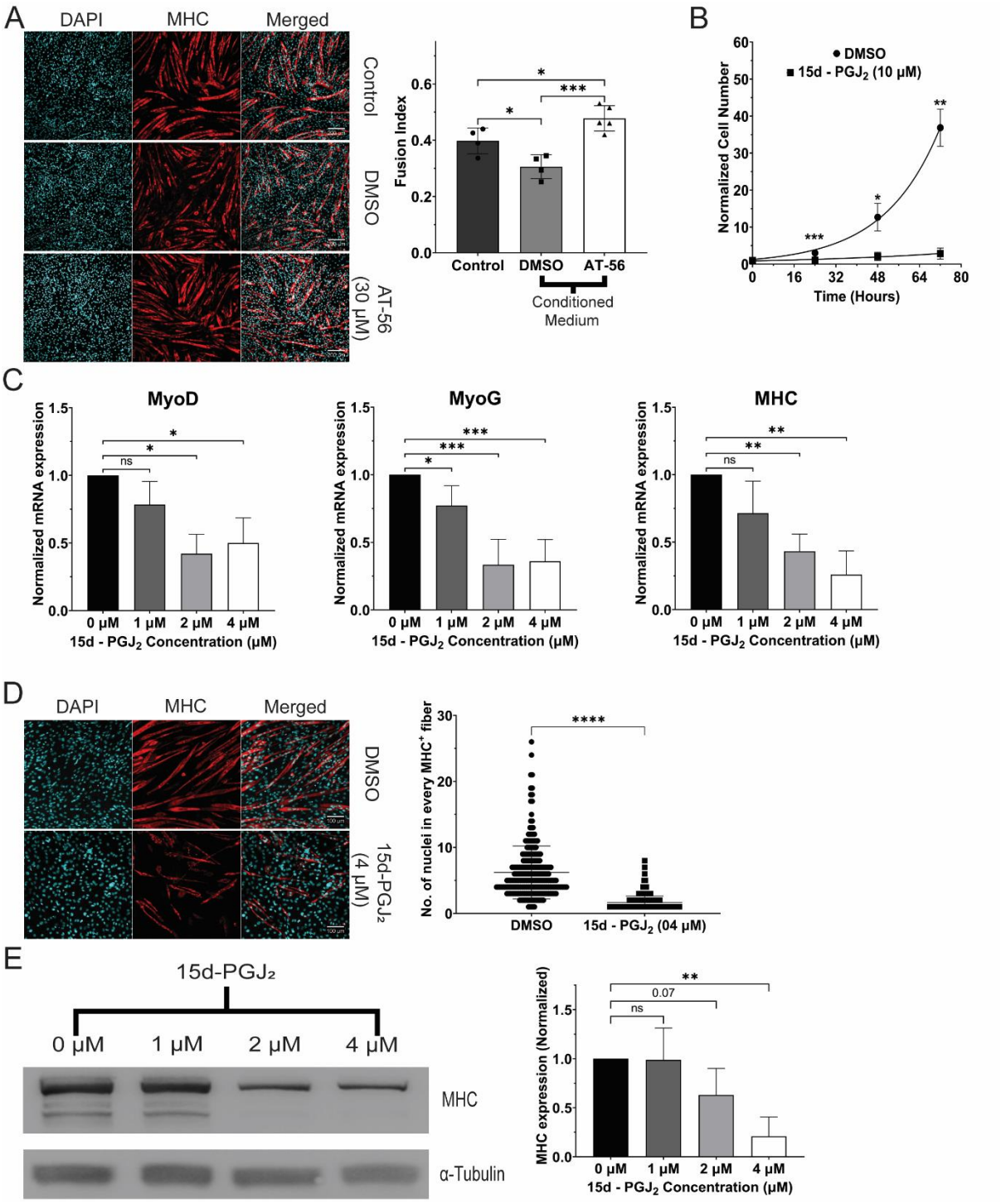

Figure 2. 15d-PGJ$_2$ inhibits differentiation of myoblasts.

A. Expression of MHC protein and the fusion of myoblasts in myotubes, measured by immunofluorescence, after treatment with conditioned medium of senescent cells treated with PTGDS inhibitor AT-56 (30 μM) or DMSO

B. Normalized number of C2C12 myoblasts treated with 15d-PGJ$_2$ (10 μM) or DMSO

C. Expression of mRNAs of markers of differentiation (MyoD, MyoG, and MHC), measured by qPCR, in C2C12 myoblasts treated with 15d-PGJ_2 (1 µM, 2 µM, or 4 µM) or DMSO.

D. Expression of MHC protein and the fusion of myoblasts in syncytial myotubes, measured by immunofluorescence, after treatment with 15d-PGJ_2 (4 µM) or DMSO.

E. Expression of MHC protein, measured by immunoblotting, in primary human skeletal myoblasts after treatment with 15d-PGJ_2 (1 µM, 2 µM, or 4 µM) or DMSO for 5 days.

(Statistical significance was tested by the two-tailed student's t-test ns=$p>0.05$, *=$p<0.05$, **=$p<0.01$, ***=$p<0.001$, ****=$p<0.0001$)

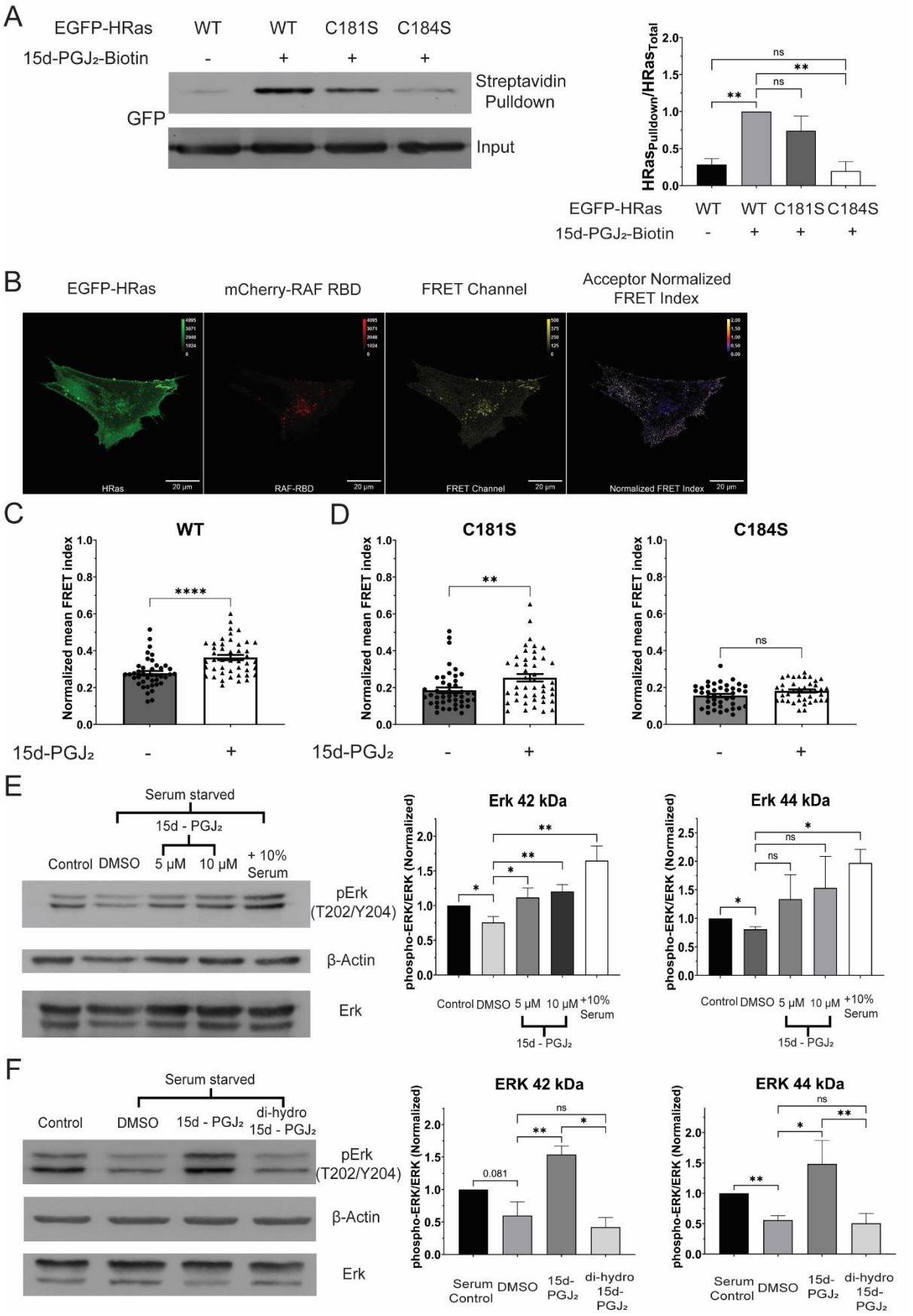

483

Figure 3. 15d-PGJ_2 covalently modifies HRas at Cysteine 184 and activates the HRas-MAPK pathway via the electrophilic cyclopentenone ring.

A. Streptavidin-immunoprecipitation of EGFP-HRas, measured by immunoblotting, in C2C12 cells after 3 hours of treatment with 15d-PGJ_2-Biotin (5 μM).
B. Representative confocal micrograph of Fluorescence Resonance Energy Transfer (FRET) between EGFP-tagged HRas (EGFP-HRas) and mCherry-tagged Ras binding domain (RBD) of RAF kinase (mCherry-RAF RBD).
C. Activation of the EGFP-tagged wild type HRas (HRas WT), measured by FRET, before and after 1 hour of treatment with 15d-PGJ_2 (10 μM) after starvation for 24 hours.
D. Activation of the EGFP-tagged C-terminal cysteine mutants of HRas (HRas C181S and HRas C184S), measured by FRET, before and after 1 hour of treatment with 15d-PGJ_2 (10 μM) after starvation for 24 hours.
E. Phosphorylation of Erk (42 kDa and 44 kDa), measured by immunoblotting, in C2C12 cells after 1 hour of treatment with 15d-PGJ_2 (5 μM, 10 μM) or DMSO after starvation for 24 hours.
F. Phosphorylation of Erk (42 kDa and 44 kDa), measured by immunoblotting, in C2C12 cells after 1 hour of treatment with 15d-PGJ_2 (10 μM)/ 9,10-dihydro-15d-PGJ_2 (10 μM) or DMSO after starvation for 24 hours.

(Statistical significance was tested by the two-tailed student's t-test ns=$p>0.05$, *=$p<0.05$, **=$p<0.01$, ***=$p<0.001$, ****=$p<0.0001$)

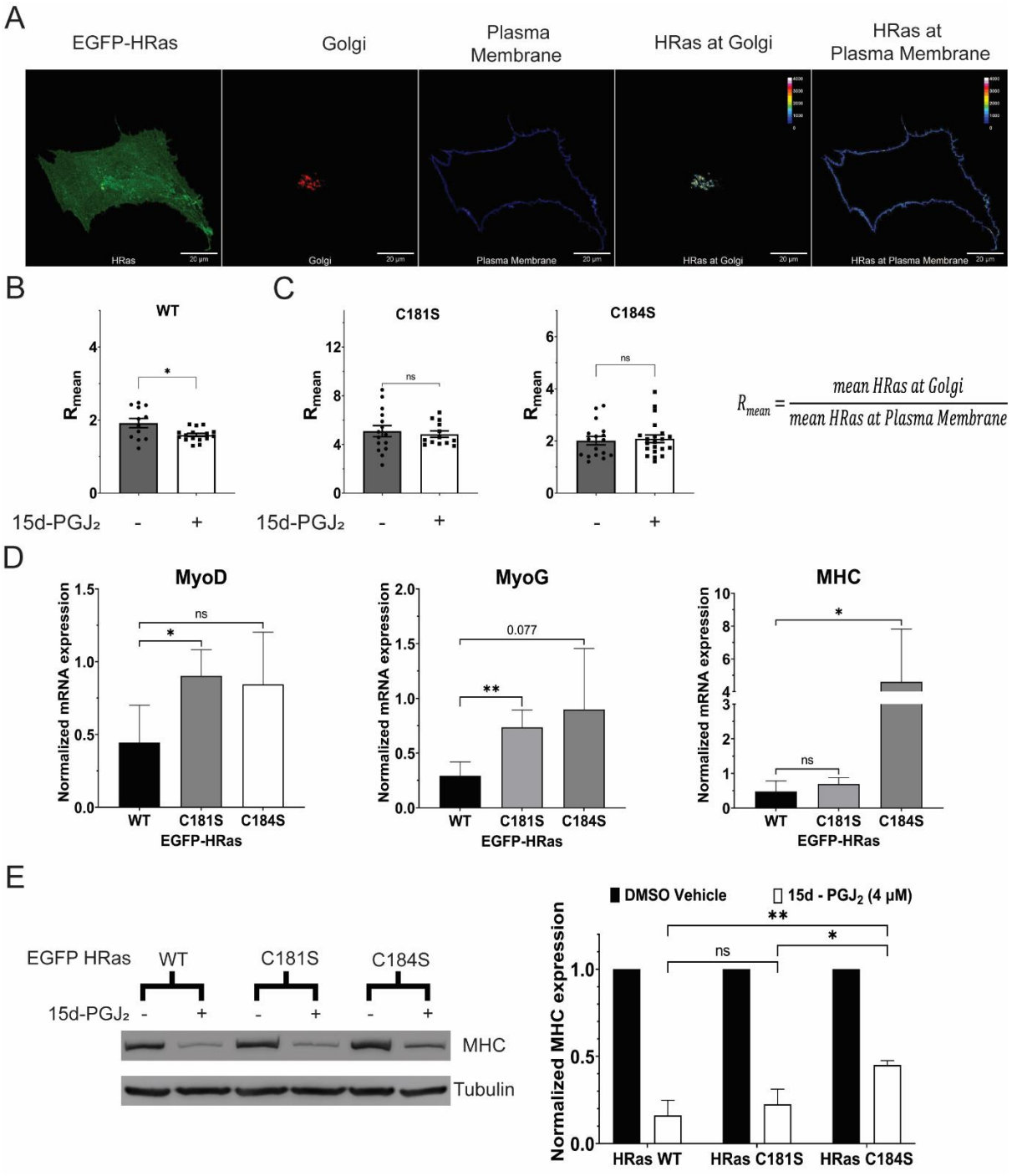

Figure 4. 15d-PGJ$_2$ controls the intracellular distribution of HRas and differentiation of C2C12 cells in an HRas C-terminal cysteine-dependent manner.

A. Representative confocal micrograph of C2C12 myoblasts showing localization of EGFP-tagged HRas between the plasma membrane (stained with Alexa Fluor 633 conjugated Wheat Germ Agglutinin) and the Golgi (labelled with TagRFP-tagged Golgi resident GalT protein). A statistic R_{mean} was defined as

514 the ratio of mean HRas intensity at the Golgi to the mean HRas intensity at the
515 plasma membrane.
516 B. Distribution of the wild-type HRas between the Golgi and the plasma
517 membrane, measured by R_{mean}, in C2C12 myoblasts treated with 15d-PGJ_2 (10
518 μM) or DMSO for 24 hours.
519 C. Distribution of the C-terminal cysteine mutants of HRas between the Golgi and
520 the plasma membrane, measured by R_{mean}, in C2C12 myoblasts treated with
521 15d-PGJ_2 (10 μM) or DMSO for 24 hours.
522 D. Expression of mRNAs of known markers of differentiation (MyoD, MyoG, and
523 MHC), measured by qPCR, in differentiating C2C12 myoblasts expressing the
524 EGFP-tagged wild-type and the C-terminal cysteine mutants of HRas after
525 treatment with 15d-PGJ_2 (4 μM) or DMSO for 5 days.
526 E. Expression of MHC protein, measured by immunoblotting, in differentiating
527 C2C12 myoblasts expressing the EGFP-tagged wild-type and the C-terminal
528 cysteine mutants of HRas after treatment with 15d-PGJ_2 (4 μM) or DMSO for 5
529 days.

530 (Statistical significance was tested by the two-tailed student's t-test ns=p>0.05,
531 *=p<0.05, **=p<0.01, ***=p<0.001, ****=p<0.0001)

Supplementary Information:

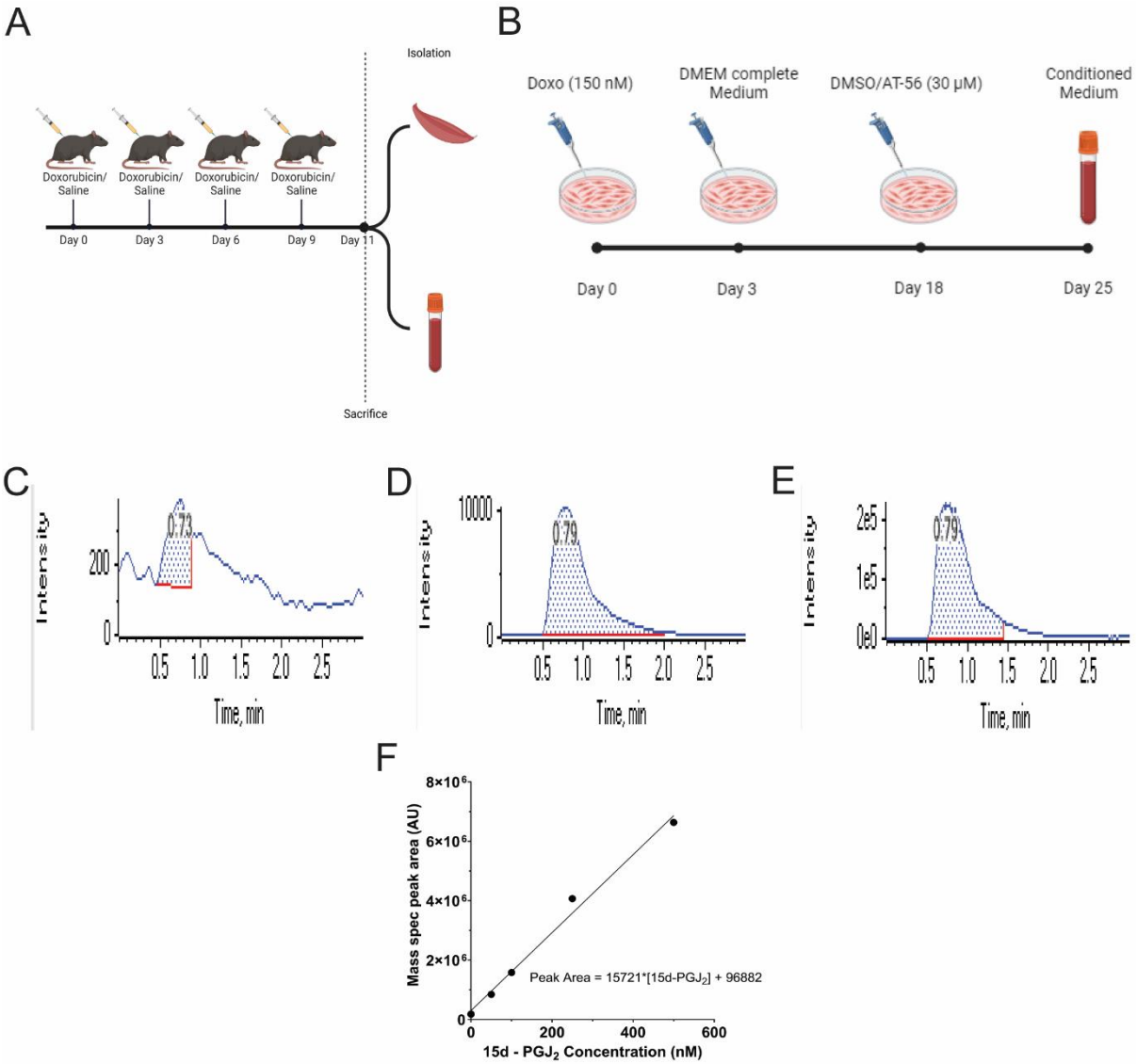

Figure S1. Treatment with Doxo induces senescence *in vivo* and *in vitro* and induces release of eicosanoid prostaglandin 15d-PGJ$_2$

A. Schematic Representation of the experimental flow for treatment of B6J mice with Doxo (5 mg/kg) or Saline.
B. Schematic representation of the experimental flow for treatment of senescent C2C12 cells with prostaglandin D synthase (PTGDS) inhibitor AT-56 (30 µM) or DMSO.
C. Representative peak of quantification of m/z 315.100 ➔ m/z 271 transitions from blank samples.

D. Representative peak of quantification of m/z 315.100 ➔ m/z 271 transitions from conditioned medium of C2C12 myoblasts treated with DMSO.

E. Representative peak of quantification of m/z 315.100 ➔ m/z 271 transitions from conditioned medium of C2C12 myoblasts treated with Doxo (150 nM).

F. Standard curve of m/z 315.100 ➔ m/z 271 fragment peak areas vs concentrations of 15d-PGJ_2

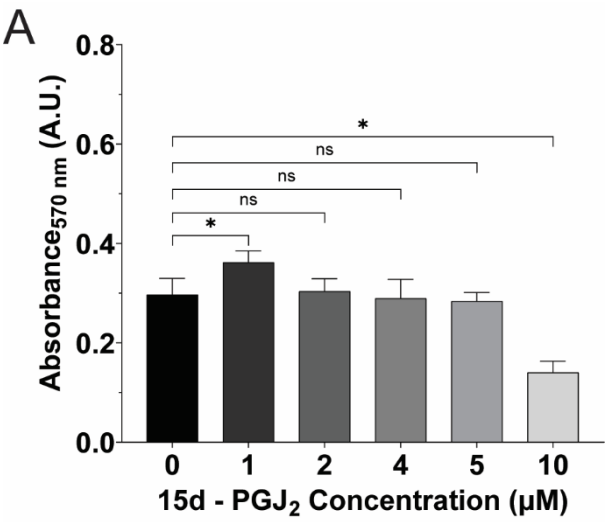

Figure S2. Viability of C2C12 myoblasts after treatment with 15d-PGJ$_2$ (10 μM) in differentiating medium.

A. Viability of C2C12 cells, measured by MTT assay, after 24 hours of treatment with 15-PGJ$_2$ (0 μM, 1 μM, 2 μM, 4 μM, 5 μM, 10 μM).

(Statistical significance was tested by the two-tailed student's t-test ns=p>0.05, *=p<0.05, **=p<0.01, ***=p<0.001, ****=p<0.0001)

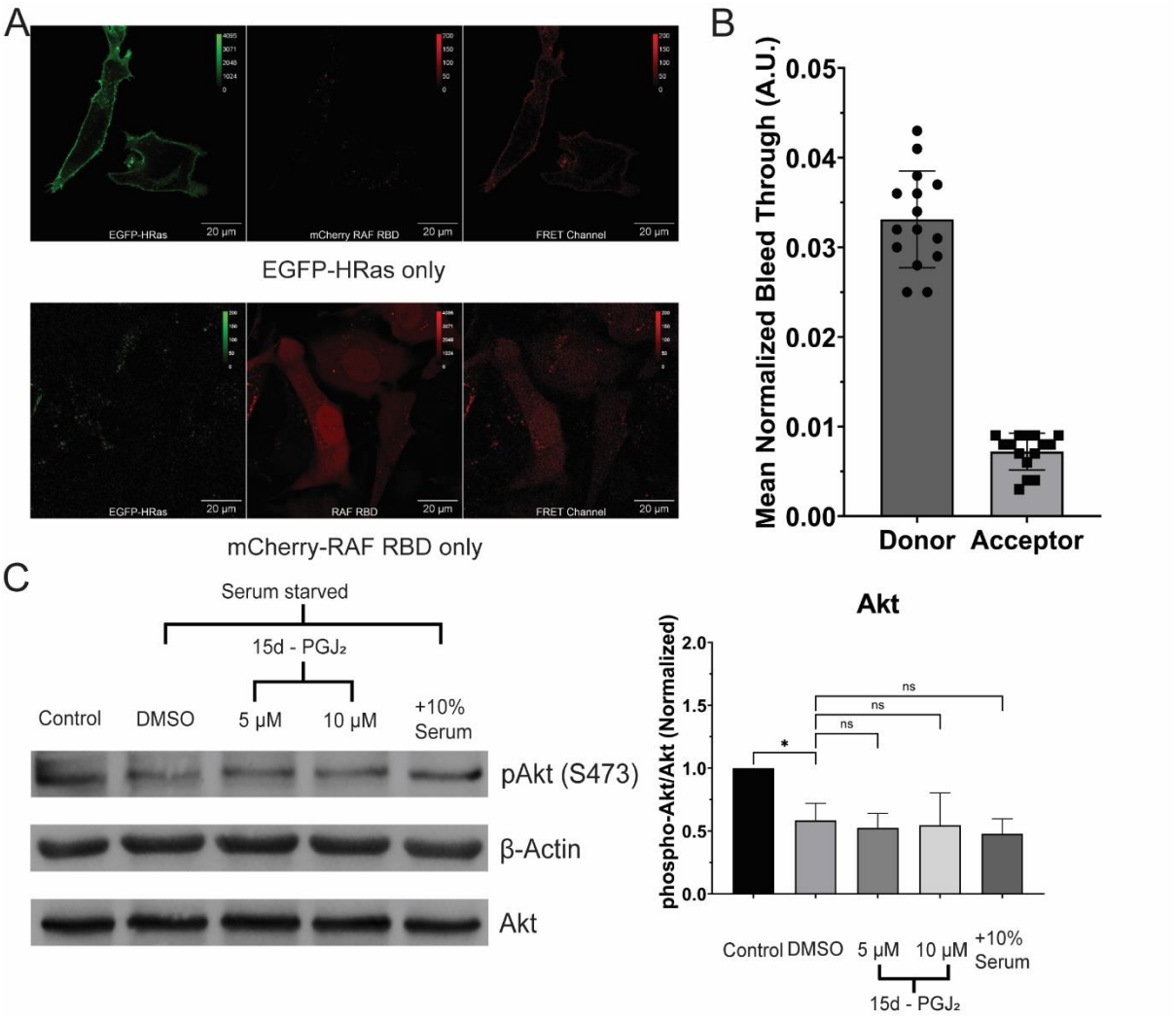

Figure S3. Activation of HRas after treatment with 15d-PGJ$_2$.

A. Representative confocal micrograph of C2C12 cells expressing only EGFP-tagged HRas or mCherry-tagged RAF RBD alone for spectral overlap (bleed-through) calculations.

B. Mean bleed-through of EGFP-tagged HRas (Donor) and mCherry-tagged RAF RBD (Acceptor) in the FRET channel.

C. Phosphorylation of Akt (measured by immunoblotting) in C2C12 cells treated with 15d-PGJ$_2$ (5, 10 µM) or DMSO for 1 hr after starving the cells in 0.2% serum medium for 24 hrs. The densitometric ratio of phosphorylated Akt (Ser473) to total Akt was normalized to non-starved C2C12 cells. (Statistical significance tested by two-tailed heteroscedastic student's t-test, N=3).

(Statistical significance was tested by the two-tailed student's t-test ns=p>0.05, *=p<0.05, **=p<0.01, ***=p<0.001, ****=p<0.0001)

570

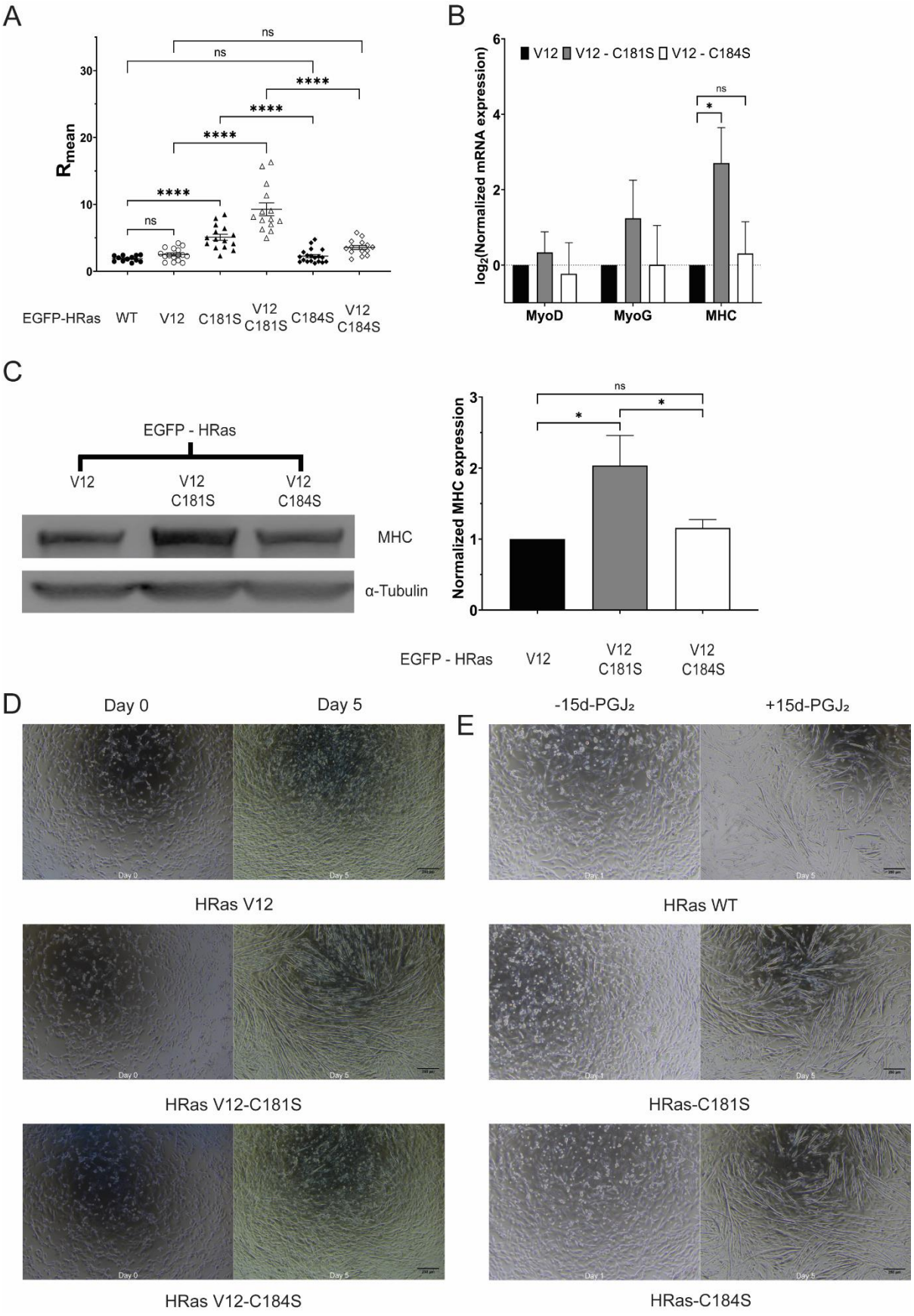

571

Figure S4. C-terminal cysteine-mediated intracellular distribution of constitutively active HRas (HRas V12) regulates the differentiation of C2C12 myoblasts.

A. Distribution of EGFP-tagged HRas WT/ HRas V12/ HRas-C181S/ HRas V12-C181S/ HRas-C184S/ HRas V12-C184S between the Golgi complex and the plasma membrane, as seen by the scatter plot of R_{mean}, the ratio of the mean HRas intensity at the Golgi complex to that at the plasma membrane, in C2C12 cells. (Statistical significance tested by two-tailed heteroscedastic student's t-test, N=3)
B. mRNA levels of MyoD, MyoG, and MyHC relative to 18s rRNA (measured by quantitative PCR) in C2C12 cells expressing EGFP-tagged HRas V12/ HRas V12-C181S/ HRas V12-C184S in C2C12 differentiation medium for 5 days. (Statistical significance tested by two-tailed heteroscedastic student's t-test, N=3)
C. Protein levels of MyHC (measured by immunoblotting) in C2C12 cells expressing EGFP-tagged HRas V12/HRas V12-C181S/HRas V12-C184S in C2C12 differentiation medium for 5 days. The densitometric ratio of levels of MyHC to α-Tubulin was normalized to C2C12 cells expressing HRas V12. (Statistical significance tested by two-tailed heteroscedastic student's t-test, N=3).
D. Brightfield image of C2C12 cells expressing EGFP-HRas V12, V12 C181S, or V12 C184S on Day 0 and Day 5 of differentiation.
E. Brightfield image of C2C12 cells expressing EGFP-HRas WT, C181S, or C184S after 5 days of treatment with 15d-PGJ_2 or DMSO.

(Statistical significance was tested by the two-tailed student's t-test ns=p>0.05, *=p<0.05, **=p<0.01, ***=p<0.001, ****=p<0.0001)

598 **Supplementary Table 1: 15d-PGJ$_2$ conc. (pmol and fg/cell) detected in samples**
599 **by mass spectrometry.**

Sample	15d-PGJ$_2$ (pmol)	Cell Number	15d-PGJ$_2$/Cell (fg)
Conditioned medium Quiescent C2C12 cells_1	27.087	462500	18.531
Conditioned medium Quiescent C2C12 cells_2	18.080	650000	8.801
Conditioned medium Senescent C2C12 cells_1	809.633	287500	891.018
Conditioned medium Senescent C2C12 cells_2	940.032	300000	991.420

600

601 **Supplementary Table 2: List of Primers:**

Primer Name	Primer Sequence (5' – 3')
HRas WT Fwd	CCGCTCGAGCTATGACGGAATATAAGCTGG
HRas WT Rev	CCGGAATTCTCAGGAGAGCACACACTTGC
HRas C181S Rev	CCGGAATTCTCAGGAGAGCACACACTTGCAGCTCATGCTGCCGG
HRas C184S Rev	CCGGAATTCTCAGGAGAGCACACACTTGCTGCTCATG
mm 18s qPCR Fwd	CCCGTTGAACCCCATTCGTG
mm 18s qPCR Rev	GGGCCTCACTAAACCATCCA
mm MyoD qPCR Fwd	TCCGCTACATCGAAGGTCTG
mm MyoD qPCR Rev	GTCCAGGTGCGTAGAAGGC
mm MyoG qPCR Fwd	CGATCTCCGCTACAGAGGC
mm MyoG qPCR Rev	GTTGGGACCGAACTCCAGT
mm MyHC qPCR Fwd	TAAACGCAAGTGCCATTCCTG
mm MyHC qPCR Rev	GGGTCCGGGTAATAAGCTGG
mm PTGS1 qPCR Fwd	TTACTATCCGTGCCAGAACCA
mm PTGS1 qPCR Rev	CCCGTGCGAGTACAATCACA
mm PTGS2 qPCR Fwd	TTCCAATCCATGTCAAAACCGT
mm PTGS2 qPCR Rev	AGTCCGGGTACAGTCACACTT
mm PTGDS qPCR Fwd	GAGTACGCTCTGCTATTCAGC
mm PTGDS qPCR Rev	GGTTGGGGCAGGAAAACAATG
mm p16 qPCR Fwd	GCTCAACTACGGTGCAGATTC
mm p16 qPCR Rev	GCACGATGTCTTGATGTCCC
mm p21 qPCR Fwd	CCTGGTGATGTCCGACCTG
mm p21 qPCR Rev	CCATGAGCGCATCGCAATC
mm p53 qPCR Fwd	CCCCTGTCATCTTTTGTCCCT
mm p53 qPCR Rev	AGCTGGCAGAATAGCTTATTGAG
mm CXCL1 qPCR Fwd	ACTGCACCCAAACCGAAGTC
mm CXCL1 qPCR Rev	TGGGGACACCTTTTAGCATCTT
mm CXCL2 qPCR Fwd	CCAACCACCAGGCTACAGG
mm CXCL2 qPCR Rev	GCGTCACACTCAAGCTCTG
mm TNF1α qPCR Fwd	CCTGTAGCCCACGTCGTAG
mm TNF1α qPCR Rev	GGGAGTAGACAAGGTACAACCC

mm IL6 qPCR Fwd	CTGCAAGAGACTTCCATCCAG
mm IL6 qPCR Rev	AGTGGTATAGACAGGTCTGTTGG
mm TGF1β qPCR Fwd	CTTCAATACGTCAGACATTCGGG
mm TGF1β qPCR Rev	GTAACGCCAGGAATTGTTGCTA

602

603 **Supplementary Table 3: List of Reagents**

Item Description	Manufacturer	Catalog No.
pEGFP-C1	Clontech	
Phusion high fidelity DNA polymerase	Thermo Scientific	F 530
Xho1 restriction enzyme	New England Biolabs Inc.	R0146
EcoR1 restriction enzyme	New England Biolabs Inc.	R0101
T4 DNA Ligase	Takara Bio	2011
DMEM High Glucose	Gibco	11995065
FBS, Certified (Origin: United States)	Gibco	16000044
Horse Serum, Heat Inactivated (Origin: New Zealand)	Gibco	26050070
Penicillin – Streptomycin – Glutamine (100x)	Gibco	10378016
Penicillin – Streptomycin (100x)	Gibco	15140163
DPBS, no calcium, no magnesium	Gibco	14190144
0.25% Trypsin - EDTA	Gibco	25200056
jetPRIME transfection reagent	Polyplus	101000046
Doxorubicin	Sigma – Aldrich	D1515
15-deoxy-$\Delta^{12,14}$-Prostaglandin J_2	Cayman Chemical Company	18570
9,10-dihydro-15-deoxy-$\Delta^{12,14}$-Prostaglandin J_2	Cayman Chemical Company	18590
15-deoxy-$\Delta^{12,14}$-Prostaglandin J_2-Biotin	Cayman Chemical Company	10141
Dynabeads™ MyOne™ Streptavidin C1	Invitrogen	65001
cOmplete Protease inhibitor cocktail tablets	Roche	11697498001
Wheat germ agglutinin, Alexa fluor 633 conjugate	Invitrogen	2307289
ProLong Gold Antifade Mounting medium	Invitrogen	P36930
Paraformaldehyde	Sigma – Aldrich	158127
TRIzol reagent	Invitrogen	15596018
PrimeScript™ 1st strand cDNA Synthesis Kit	Takara Bio	6110A
PowerUp™ SYBR™ Green Master Mix	Applied Biosystems	A25742
WesternBrightTM ECL-spray Western blotting detection system	advansta	K-12049-D50

Fetuin (Bovine)	Sigma – Aldrich	F2379
hEGF	Sigma – Aldrich	E9644
N2 Supplement	Thermo Scientific	17502048
Dexamethasone	Sigma – Aldrich	D4902
DMEM Low Glucose	Thermo Scientific	10567014
Bovine Serum Albumin Fraction-V, Cell culture tested	HIMEDIA	9048468
Pierce^{TM} Streptavidin Magnetic Beads	Thermo Scientific	88816

604

605 **Supplementary table 4: List of Antibodies**

Antibody Name	Clonality	Species of Origin	Manufacturer	Catalog No.
Phospho-Erk (Thr202/ Tyr204)	Polyclonal	Rabbit	Cell Signaling Technology	9101S
Erk	Polyclonal	Rabbit	Cell Signaling Technology	9102S
GAPDH	Monoclonal	Mouse	Puregene	PG23002
β-actin	Polyclonal	Rabbit	Cell Signaling Technology	4967S
Phospho-Akt (Ser473)	Monoclonal	Mouse	Cell Signaling Technology	4051S
Akt	Monoclonal	Rabbit	Cell Signaling Technology	4691S
GFP	Monoclonal	Rabbit	Cell Signaling Technology	2956S
Myosin Heavy Chain	Monoclonal	Mouse	Invitrogen	14-6503-82
Myosin Heavy Chain	Monoclonal	Mouse	Developmental Studies Hybridoma Bank (DSHB)	MF20
p21	Monoclonal	Mouse	Santacruz Biotechnology	sc-6246
γH2A.X	Polyclonal	Rabbit	Novus Biologicals	NB100384
Tubulin	Monoclonal	Mouse	Cell Signaling Technology	3873S
HRP - Anti-Mouse		Horse	Cell Signaling Technology	7076S
HRP - Anti-Rabbit		Goat	Cell Signaling Technology	7074P2
Alexa Fluor 568 – Anti-Mouse	Polyclonal	Goat	Invitrogen	A11031

606

Materials and Methods

Plasmids

Unmutated and cysteine mutants of HRas WT [HRas WT, HRas-C181S, and HRas-C184S] and HRas V12 [HRas V12, HRas V12-C181S, HRas V12-C184S] were cloned in the pEGFPC1 vector (Clontech) by restriction digestion-ligation method. Constructs of wild-type HRas were PCR amplified from a previously available HRas construct in the lab with construct-specific primers. Proper nucleotide additions were made to the forward primer to maintain the EGFP ORF, marking a 7 amino acid linker between the proteins. The construct sequences were confirmed by Sanger sequencing. GalT-TagRFP construct was a gift from Prof. Satyajit Mayor and was used to mark the Golgi. mCherry-RAF-RBD construct was a gift from Prof. Phillipe Bastiens and was used to measure the activity of HRas GTPase using FRET.

Cell Maintenance

C2C12 mouse myoblasts (CRL–1772) were obtained from ATCC and were maintained in DMEM complete medium @ 37° C, 5% CO_2. For experiments, the cells were trypsinized with 0.125% trypsin-EDTA (Gibco) and were seeded in required numbers in cell culture dishes. Human Skeletal Muscle Myoblast (CC-2580) were obtained from Lonza and were maintained in DMEM Skeletal Muscle growth medium @ 37° C, 5% CO_2. For experiments, the cells were trypsinized with 0.125% trypsin – EDTA (Gibco) and were seeded in required numbers in cell culture dishes. All cultures tested negative for mycoplasma checked by Mycoalert Mycoplasma Detection Kit (Lonza).

Conditioned media collection

C2C12 cells seeded in 60mm dishes were treated with Doxorubicin (150 nM) for 3 days. The media was then changed to DMEM complete medium without Doxorubicin for 19 days after treatment with Doxorubicin. The cells were treated with DMSO or AT-56 (30 μM) in the DMEM complete medium for 2 days. On Day 21, the cells were treated with DMSO or At-56 in DMEM Starvation medium for 3 days. The media was then collected and centrifuged @1000g, R.T. for 5 minutes. The media was then stored at -80° C after flash freezing in liq. N_2 till further requirement.

Treatments

15d-PGJ_2 (Cayman Chemical Company) dissolved in DMSO (10 mM) was diluted in DMEM media for experiments. 9,10-dihydro-15d-PGJ_2 (Cayman Chemical Company) dissolved in DMSO (10 mM) was appropriately diluted in DMEM media for experiments. DMSO was used as vehicle control. A media change of the same composition was given every 24 hours. C2C12 cells with 70-80% confluency were treated with Doxorubicin (Doxo) for 3 days. After 72 hours, Doxo was removed from the medium and the cells were kept for 10 more days with media change every 3 days till the end of the experiment. C2C12 cells transfected with EGFP-HRas WT/C181S/C184S in 35mm dishes were treated with 15d-PGJ_2-Biotin (5 µM) in DMEM Hi Glucose medium (Gibco) supplemented with 1% Penicillin-streptomycin-Glutamine (Gibco) without fetal bovine serum for 3 hours. Conditioned medium collected from senescent cells was thawed @ 37° C. The medium was then supplemented with 2% heat-inactivated horse serum and 1% penicillin-streptavidin-glutamine. C2C12 myoblasts were treated with the conditioned medium and were given a media change every 48 hours.

Transfections:

C2C12 cells were seeded in 35 mm dishes to achieve confluency of ~60-70%. For western blot, immunoprecipitation, and differentiation experiments, the cells were transfected with EGFP-tagged HRas WT/ HRas-C181S/ HRas-C184S/ HRas V12/ HRas V12-C181S/ HRas V12-C184S using the jetPRIME transfection reagent (Polyplus) using the manufacturer's protocol. For measuring the intracellular distribution of HRas, the cells were reverse transfected with EGFP-tagged HRas WT/ HRas-C181S/ HRas-C184S/ HRas V12/ HRas V12-C181S/ HRas V12-C184S and GalT-TagRFP, a Golgi apparatus marker protein tagged with red fluorescent TagRFP protein using the jetPRIME transfection reagent using the manufacturer's protocol. For measuring the activity of HRas, the cells seeded in imaging dishes (iBidi) were transfected with EGFP-HRas and mCherry-RAF-RBD using jetPRIME transfection reagent (Polyplus) using the manufacturer's protocol. Transfection efficiency was confirmed by checking for GFP and RFP fluorescence after 24 hours of transfection.

Myoblast differentiation

C2C12 cells were treated with either 15d-PGJ_2 or DMSO in the C2C12 differentiation medium. The cells were given a media change of the same composition every 24

hours. The cells were harvested after 5 days of 15d-PGJ_2 treatment for either RNA or protein isolation. Human Skeletal Muscle Myoblast cells were treated with DMSO or 15d-PGJ_2 in the Skeletal Muscle Differentiation medium. A media change of the same composition was given every 24 hours. The cells were harvested after 5 days of treatment for protein isolation.

X-Gal staining

Proliferative and Doxo-treated C2C12 cells were fixed with 0.25% glutaraldehyde, washed with PBS, and incubated overnight in X-gal staining solution at 37° C in a CO_2-free chamber. The presence of the Indigo blue product was confirmed using the Ti2 widefield inverted microscope (Nikon).

Immunoprecipitation

C2C12 cells transfected with EGFP-HRas and treated with 15d-PGJ_2-Biotin were harvested and lysed in RIPA-PP buffer and the lysate was centrifuged @15000 rpm, 4° C, 30 minutes. Protein estimation was done using the BCA assay kit (G Biosciences). 100 µg of protein was loaded on 10 µl MyOne Streptavidin C1 dynabeads blocked with 1% BSA in IP washing buffer. The lysate-streptavidin mix was incubated @4° C, 10 rpm overnight. The beads were then washed with IP washing buffer and then boiled in 20 µl Laemmlli buffer. 15 µl of the beads were loaded on 12% SDS-Polyacrylamide gel for detection of EGFP-HRas by immunoblotting using EGFP antibody.

Western blotting

For measuring Erk/Akt phosphorylation in C2C12 cells were seeded in 35 mm dishes. 1x 35 mm dish was harvested in RIPA – PP the next day, while the rest were incubated in DMEM starvation medium @37° C. The cells were treated with 15d - PGJ_2 after 24 hrs of starvation @37° C. The cells were harvested at 1 hour after treatment in RIPA-PP. Protein quantification was done using BCA assay (G Biosciences) using the manufacturer's protocol. An equal mass of proteins was loaded onto a 12% SDS Polyacrylamide gel in Laemmlli buffer. The proteins were transferred onto a PVDF membrane and were probed with phospho-Erk/Erk antibodies for measuring Erk phosphorylation and with phospho-Akt/Akt antibodies for measuring Akt phosphorylation. For measuring the expression of Myosin heavy chain, C2C12 cells

expressing EGFP-tagged HRas WT/ HRas-C181S/ HRas-C184S/ HRas V12/ HRas V12-C181S/ HRas V12-C184S or Human Skeletal Muscle Myoblasts were seeded in 35 mm dishes and were harvested in RIPA-PP after 5 days of differentiation. Protein quantification was done using BCA assay (G Biosciences) using the manufacturer's protocol. An equal mass of proteins was loaded onto an 8% SDS Polyacrylamide gel in Laemmlli buffer. The proteins were transferred onto a PVDF membrane and were probed with Myosin Heavy Chain Antibody.

qPCR

C2C12 cells, untransfected or expressing EGFP-tagged HRas WT/ HRas-C181S/ HRas-C184S and treated with DMSO/15d - PGJ_2, or expressing EGFP-tagged HRas V12/ HRas V12-C181S/ HRas V12-C184S were lysed in TRIZol at the end of the experiment (Invitrogen). RNA was isolated from the lysate by the chloroform-isopropanol method using the manufacturer's protocol. The RNA was quantified and 1.5 µg of RNA was used to prepare cDNA using PrimeScript 1st strand cDNA Synthesis Kit (Takara Bio) and random hexamer primer. Gene expression for differentiation markers was measured by qPCR using PowerUp™ SYBR™ Green Master Mix (Applied Biosystems) and previously reported qPCR primers (Wang et al., 2012). Relative gene expression was quantified using the $\Delta\Delta C_T$ method (Livak and Schmittgen 2001) with 18s rRNA as an internal loading control and DMSO vehicle as an experimental control.

Immunofluorescence

C2C12 cells were seeded in 35 mm dishes (Corning) on glass coverslips (Blue Star) coated with 0.2% Gelatin (Porcine, Sigma Aldrich) and were fixed with the fixative solution at the end of the experiment. The cells were then permeabilized and blocked with the blocking solution and were then incubated with Myosin Heavy Chain antibody in the blocking solution overnight. The cells were then washed with 1x PBS, incubated with fluorophore tagged secondary antibody, and were mounted in Prolong gold antifade medium with DAPI (Invitrogen). The cells were then imaged under the FV3000 inverted confocal laser scanning microscope (Olympus-Evident) using appropriate lasers and detectors.

Confocal microscopy for measuring HRas distribution between the Golgi and the plasma membrane

C2C12 cells expressing EGFP-tagged HRas WT/ HRas-C181S/ HRas-C184S + GalT-TagRFP were starved overnight in DMEM starvation medium and treated with DMSO or 15d-PGJ_2 (10 μM) in DMEM complete medium for 24 hrs, with a medium change @ 12 hrs post-treatment. The cells were then fixed with the fixative solution @ R. T., washed with PBS, and stained for plasma membrane with Alexa Fluor 633 conjugated Wheat Germ Agglutinin (WGA-633) (Invitrogen). The cells were washed with PBS and were then mounted on glass slides in ProLong Gold Antifade Mounting medium (Invitrogen). C2C12 cells expressing EGFP-tagged HRas V12/ HRas V12-C181S/ HRas V12-C184S were also fixed with the fixative solution @R. T., washed with PBS, stained with WGA-633, and mounted on slides in Prolong gold antifade medium (Invitrogen). The cells were imaged with the FV3000 inverted confocal laser scanning microscope (Olympus-Evident) using appropriate lasers and detectors. Preliminary image processing was done using ImageJ (NIH), while batch analysis of HRas at the plasma membrane and the Golgi complex was done using a custom MATLAB script, where EGFP-HRas image was overlayed onto the GalT-TagRFP and WGA-633 image to obtain HRas localization at the Golgi complex and the Plasma Membrane respectively. A ratio of mean HRas intensity at the Golgi complex to that of at the Plasma membrane (R_{mean}) was calculated and was used to compare HRas distribution between treatments.

FRET confocal microscopy to measure the intracellular activity of HRas

C2C12 cells expressing EGFP-tagged HRas WT/HRas C181S/HRas C184S and mCherry-RAF-RBD were starved overnight in the DMEM starvation medium. The cells were imaged with the FV3000 inverted confocal laser scanning microscope (Olympus-Evident) using the following lasers and detectors:

1. Donor Channel: 488nm excitation, 510 (+/-) 20nm detection.
2. Acceptor Channel: 561nm excitation, 630 (+/-) 50nm detection.
3. FRET Channel: 488nm excitation, 630 (+/-) 50nm detection.

The cells were then treated with 15d-PGJ_2 (10 μM) for 1 hour and were imaged using the same imaging parameters. C2C12 cells expressing EGFP-HRas or mCherry-RAF RBD only were used to calculate the bleed-through corrections (EGFP emission @ 630 (+/-) 50nm, and Excitation of mCherry by 488 nm laser). Preliminary processing was done using ImageJ (NIH). The FRET index was calculated using the FRET and

co-localization analyzer plugin(Hachet-Haas et al., 2006). The FRET index was then divided by the intensity of the Acceptor channel to normalize the variation in the expression of mCherry. We used the mean normalized FRET index to compare the activity of HRas before and after treatment with 15d-PGJ_2.

Quantification of myotube fusion index

Differentiated C2C12 myoblasts were immunostained for MHC and DAPI and were imaged on the FV3000 inverted confocal laser scanning microscope (Olympus-Evident). Analysis of the fusion index was done using the Myotube Analyzer Software(Noë et al., 2022). DAPI and MHC images were thresholded to remove background noise. The images were converted to binary masks and the channels were overlayed to obtain the no. of nuclei overlaying with MHC^{+ve} fibers. The fusion index was calculated as the percentage ratio of no. nuclei overlaying the MHC^{+ve} fibers to the total no. of nuclei in the field of view.

Quantification of cell doubling time

Cells were counted every 24 hours and the normalization was done to the number of cells counted on day 0 of the treatment (to consider attaching efficiency and other cell culture parameters). Doubling time was calculated as the reciprocal of the slope of the graph of log2(normalized cell number) vs time.

MTT Assay

An equal number of C2C12 cells were seeded in 96 well plates in replicates. MTT assay was done at the end of the experiment using the manufacturer's protocol. MTT reagent (Sigma Aldrich) was dissolved in 1x DPBS (5 mg/ml) and was filter sterilized. MTT reagent was added to each well and the cells were incubated @37° C, 5% CO_2 for 3 hours. The medium was removed at the end of the incubation and the precipitated crystals were dissolved in DMSO @37° C, 5% CO_2 for 15 minutes. Absorbance @570 nm was recorded using the varioskan multimode plate reader (Thermo Scientific).

Animal Experiments

Mice were maintained at BLiSC Animal Care and Resource Centre (ACRC). All the procedures performed were approved by the Internal Animal Users Committee (IAUC) and the Institutional Animal Ethics Committee (IAEC). 12–15-week-old C57BL/6J

(JAX#000664) mice were injected intraperitoneally (I.P.) with 5 mg/kg Doxorubicin (Doxo) four times, once every three days. Intraperitoneal injection of Saline was used as a control. The mice were sacrificed on Day 11 after the first injection. Hindlimb muscles from 4 animals (control and treated with Doxo each) were used for qPCR analysis and Hindlimb muscles from 3 animals (control and treated with Doxo each) were used for immunohistochemical analysis.

Lipid extraction and detection of 15d-PGJ$_2$ by mass spectrometry

For lipid extraction, cell pellets were resuspended in 3ml of a methanol solvent [water: methanol: 2:1, 1% formic acid (FA)] whereas only 1 ml of methanol with 3% FA was added to the 2 ml of CM, making a uniform sample volume of 3 ml. Subsequently, 1 ml of ethyl acetate was added to each sample and mixed vigorously. Phase separation was done by centrifuging the mixture (12000xg, 4℃ for 10 mins), and the organic phase containing the lipid was collected. This process was repeated thrice in total and all the organic phases were combined and dried under a nitrogen stream at RT. The residues were resuspended in 100 µl of 50% acetonitrile in water with 0.1% FA and were subjected to mass spec analysis using the Waters® Acquity UPLC class I system The detection of 15d-PGJ$_2$ was performed using an electrospray ionization source (ESI) operating in the negative ion mode and a quadrupole trap mass spectrometer (AB SCIEX QTRAP 6500) connected to a Waters® Acquity UPLC class I system (Waters, Germany) outfitted with a binary solvent delivery system with an online degasser and a column manager with a column oven coupled to a UPLC autosampler. 5 µl samples were injected into the union for analysis. Solvent A consisted of 0.1% ammonium acetate in water and solvent B was 0.1% ammonium acetate in a mixture of acetonitrile/water (95:5). For each run, the LC gradient was: 0 min, 20% B; 0.5 min, 20% B; 1.5 min, 90% B; 2.5 min, 20% B; 3min, 20% B. Analyte detection was performed using multiple reaction monitoring (MRM), 315.100 ➔ 271.100 and 315.100 ➔ 203.100. Source parameters were set as follows: capillary voltage 3.8 kV, desolvation gas flow 25 L/h, source temperature 350 °C, ion source gas 1 flow 40 L/h, and ion source gas 2 flow 40 L/h. Acquisition and quantification were completed with Analyst 1.6.3 and Multiquant 3.0.3, respectively (method adopted from (Morgenstern et al., 2018)). For the standards, 2ml media of different known concentrations (50nM, 100nM, 250nM, and 500nM) of 15d-PGJ$_2$ were prepared and subjected to the same

826 extraction procedure as that of CM. A standard curve was plotted with the known
827 concentration and the mass spec peak area, and the concentration of the lipid in
828 samples was calculated.

Reagents

- DMEM complete medium: DMEM Hi Glucose medium (Gibco) supplemented with 1% Penicillin – Streptomycin – Glutamine (Gibco) and heat-inactivated 10% Fetal Bovine Serum (US origin) (Gibco).
- Basal Conditioned medium: DMEM Hi Glucose medium (Gibco) supplemented with 1% Penicillin – Streptomycin – Glutamine (Gibco) and heat-inactivated 2% Fetal Bovine Serum (US origin) (Gibco).
- C2C12 differentiation medium: DMEM Hi Glucose medium (Gibco) supplemented with 2% Horse Serum (Gibco) and 1% Penicillin – Streptomycin – Glutamine (Gibco).
- DMEM Starvation medium: DMEM Hi Glucose medium (Gibco) supplemented with 0.2%heat-inactivated fetal bovine serum (US origin) (Gibco) and 1% Penicillin – Streptomycin – Glutamine (Gibco).
- RIPA – PP buffer: RIPA buffer (Invitrogen) supplemented with protease inhibitor cocktail (Roche) and 5 mM Sodium Fluoride and 5 mM Sodium Orthovanadate.
- TBS – T buffer: 50 mM Tris-Cl (pH = 7.5), 150 mM NaCl and 0.1% Tween – 20 in water.
- PBS: 2.67 mM KCl, 1.47 mM KH_2PO_4, 137.93 mM NaCl, 8.06 mM Na_2HPO_4 in water.
- IP Washing Buffer: 150 mM NaCl, 0.1% SDS, 1% NP-40 in 50 mM Tris-Cl (pH=7)
- Fixative Solution: 4% (w/v) Paraformaldehyde (Sigma – Aldrich) in PBS.
- Blocking Solution: 2% Heat Inactivated FBS, 0.2% BSA, 0.2% Triton - X, 0.05% NaN_3 in PBS.
- Skeletal Muscle Growth Medium: DMEM Low Glucose Medium (Gibco), supplemented with 1% Penicillin – Streptomycin – Glutamine (Gibco), heat-inactivated 10% Fetal Bovine Serum (US origin) (Gibco), Bovine Fetuin (50 µg/ml) (Sigma – Aldrich), Dexamethasone (0.4 µg/ml), and hEGF (10 ng/ml).
- Skeletal Muscle Differentiation Medium: DMEM low glucose medium (Gibco) supplemented with 2% Horse Serum, 1% Penicillin – Streptomycin (Gibco), and 1% N2 Supplement.

Acknowledgments

We thank Prof. Satyajit Mayor (NCBS), Prof. Phillipe Bastiens, and Prof. Apurva Sarin (InStem) for providing the wid-type HRas construct, the mCherry-RAF RBD construct and the vector backbones respectively. We thank Dr. Neetu Saini (InStem) for her help with setting up the cell culture facility. We thank Mr. Heera Lal for his help with the animal work. We thank Dr. Kamlesh Kumar Yadav and Ms. Sudeshna Saha for their help during the project. We thank the Central Imaging and Flow Cytometry Facility (CIFF) (NCBS-InStem) for their support with microscopy. We thank the Animal Care and Resource Centre (ACRC) (NCBS-InStem) for their support with mouse experiments. We thank the Mass Spectrometry facility (NCBS-InStem) for their support with the mass spectrometry work.

Funding

This work was supported by SERB SUPRA grant to Dr. Arvind Ramanathan. SSP and AB are supported by GS program (InStem), AV is supported by DBT-JRF grant.

Author Contribution

SSP: Project conceptualization, Cell culture treatments and assays, Biochemistry, Microscopy, Image Processing, and analysis, Writing: original draft, review, and edits.

AB: Animal work, Cell culture treatments and assays, Biochemistry, Mass Spectrometry, Writing: review and edits.

AV: Cell culture treatments and assays, Image processing and analysis, writing: review and edits.

SSS: Cell culture treatments and assays, Biochemistry, Writing: review and edits.

MAJ: Image processing and analysis.

RGHM: Mass Spectrometry.

AR: Project Conceptualization, Writing: original draft, review, and edits. Corresponding Author.

Competing Interests

The authors declare no competing interests.

888 **References**

889 Agudo-Ibáñez L, Herrero A, Barbacid M, Crespo P. 2015. H-Ras Distribution and
890 Signaling in Plasma Membrane Microdomains Are Regulated by Acylation and
891 Deacylation Events. *Mol Cell Biol* **35**:1898–1914. doi:10.1128/mcb.01398-14

892 Bennett AM, Tonks NK. 1997. Regulation of distinct stages of skeletal muscle
893 differentiation by mitogen-activated protein kinases. *Science (80-)* **278**:1288–
894 1291. doi:10.1126/SCIENCE.278.5341.1288

895 Bihani T, Chicas A, Lo CPK, Lin AW. 2007. Dissecting the senescence-like program
896 in tumor cells activated by ras signaling. *J Biol Chem* **282**:2666–2675.
897 doi:10.1074/jbc.M608127200

898 Bihani T, Mason DX, Jackson TJ, Chen SC, Boettner B, Lin AW. 2004. Differential
899 Oncogenic Ras Signaling and Senescence in Tumor Cells. *Cell Cycle* **3**:1201–
900 1207.

901 Bittles AH, Harper N. 1984. Increased glycolysis in ageing cultured human diploid
902 fibroblasts. *Biosci Rep* **4**:751–756. doi:10.1007/BF01128816

903 Busquets-Hernández C, Triola G. 2021. Palmitoylation as a Key Regulator of Ras
904 Localization and Function. *Front Mol Biosci* **8**:1–8.
905 doi:10.3389/fmolb.2021.659861

906 Calabrese V, Mallette FA, Deschênes-Simard X, Ramanathan S, Gagnon J, Moores
907 A, Ilangumaran S, Ferbeyre G. 2009. SOCS1 Links Cytokine Signaling to p53 and
908 Senescence. *Mol Cell* **36**:754–767. doi:10.1016/j.molcel.2009.09.044

909 Campisi J. 2005. Senescent cells, tumor suppression, and organismal aging: Good
910 citizens, bad neighbors. *Cell* **120**:513–522. doi:10.1016/j.cell.2005.02.003

911 Casar B, Badrock AP, Jiménez I, Arozarena I, Colón-bolea P, Lorenzo-martín LF,
912 Barinaga-rementería I, Barriuso J, Cappitelli V, Donoghue DJ, Bustelo XR,
913 Hurlstone A, Crespo P. 2018. RAS at the Golgi antagonizes malignant
914 transformation through PTPR κ -mediated inhibition of ERK activation. *Nat*
915 *Commun* 1–17. doi:10.1038/s41467-018-05941-8

916 Chen Q, Ames BN. 1994. Senescence-like growth arrest induced by hydrogen
917 peroxide in human diploid fibroblast F65 cells. *Proc Natl Acad Sci U S A* **91**:4130–

4134. doi:10.1073/pnas.91.10.4130

Chen QM, Bartholomew JC, Campisi J, Acosta M, Reagan JD, Ames BN. 1998. Molecular analysis of H2O2-induced senescent-like growth arrest in normal human fibroblasts: p53 and Rb control G1 arrest but not cell replication. *Biochem J* **332**:43–50. doi:10.1042/bj3320043

Chen YX, Zhong XY, Qin YF, Bing W, He LZ. 2003. 15d-PGJ2 inhibits cell growth and induces apoptosis of MCG-803 human gastric cancer cell line. *World J Gastroenterol* **9**:2149. doi:10.3748/WJG.V9.I10.2149

Childs BG, Durik M, Baker DJ, van Deursen JM. 2015. Cellular senescence in aging and age-related disease: from mechanisms to therapy disease: from mechanisms to therapy. doi:10.1038/nm.4000

Choi J, Suh J-Y, Kim D-H, Na H-K, Surh Y-J. 2020. 15-Deoxy-Δ12,14-prostaglandin J2 Induces Epithelial-tomesenchymal Transition in Human Breast Cancer Cells and Promotes Fibroblast Activation. *J Cancer Prev* **25**:152–163. doi:10.15430/JCP.2020.25.3.152

Conte TC, Duran-Bishop G, Orfi Z, Mokhtari I, Deprez A, Côté I, Molina T, Kim TY, Tellier L, Roussel MP, Maggiorani D, Benabdallah B, Leclerc S, Feulner L, Pellerito O, Mathieu J, Andelfinger G, Gagnon C, Beauséjour C, McGraw S, Duchesne E, Dumont NA. 2023. Clearance of defective muscle stem cells by senolytics restores myogenesis in myotonic dystrophy type 1. *Nat Commun 2023 141* **14**:1–17. doi:10.1038/s41467-023-39663-3

Coppé JP, Desprez PY, Krtolica A, Campisi J. 2010. The senescence-associated secretory phenotype: The dark side of tumor suppression. *Annu Rev Pathol Mech Dis* **5**:99–118. doi:10.1146/annurev-pathol-121808-102144

Coppé JP, Patil CK, Rodier F, Sun Y, Muñoz DP, Goldstein J, Nelson PS, Desprez PY, Campisi J. 2008. Senescence-associated secretory phenotypes reveal cell-nonautonomous functions of oncogenic RAS and the p53 tumor suppressor. *PLoS Biol* **6**. doi:10.1371/journal.pbio.0060301

Cosgrove BD, Gilbert PM, Porpiglia E, Mourkioti F, Lee SP, Corbel SY, Llewellyn ME, Delp SL, Blau HM. 2014. Rejuvenation of the muscle stem cell population restores

948 strength to injured aged muscles. *Nat Med 2014 203* **20**:255–264.
949 doi:10.1038/nm.3464

950 D'Adda Di Fagagna F. 2008. Living on a break: Cellular senescence as a DNA-
951 damage response. *Nat Rev Cancer* **8**:512–522. doi:10.1038/nrc2440

952 D'Adda Di Fagagna F, Reaper PM, Clay-Farrace L, Fiegler H, Carr P, Von Zglinicki T,
953 Saretzki G, Carter NP, Jackson SP. 2003. A DNA damage checkpoint response
954 in telomere-initiated senescence. *Nature* **426**:194–198. doi:10.1038/nature02118

955 Davalos AR, Coppe JP, Campisi J, Desprez PY. 2010. Senescent cells as a source of
956 inflammatory factors for tumor progression. *Cancer Metastasis Rev* **29**:273–283.
957 doi:10.1007/s10555-010-9220-9

958 Davis M, Malcolm S, Hall A, Marshall CJ. 1983. Localisation of the human N-ras
959 oncogene to chromosome 1cen - p21 by in situ hybridisation. *EMBO J* **2**:2281–
960 2283. doi:10.1002/J.1460-2075.1983.TB01735.X

961 de Lima Junior EA, Yamashita AS, Pimentel GD, De Sousa LGO, Santos RVT,
962 Gonçalves CL, Streck EL, de Lira FS, Rosa Neto JC. 2016. Doxorubicin caused
963 severe hyperglycaemia and insulin resistance, mediated by inhibition in AMPk
964 signalling in skeletal muscle. *J Cachexia Sarcopenia Muscle* **7**:615–625.
965 doi:10.1002/JCSM.12104

966 Di Leonardo A, Linke SP, Clarkin K, Wahl GM. 1994. DNA damage triggers a
967 prolonged p53-dependent G1 arrest and long-term induction of Cip1 in normal
968 human fibroblasts. *Genes Dev* **8**:2540–2551. doi:10.1101/gad.8.21.2540

969 Dilley TK, Bowden GT, Chen QM. 2003. Novel mechanisms of sublethal oxidant
970 toxicity: Induction of premature senescence in human fibroblasts confers tumor
971 promoter activity. *Exp Cell Res* **290**:38–48. doi:10.1016/S0014-4827(03)00308-2

972 Dimri GP, Leet X, Basile G, Acosta M, Scorrt G, Roskelley C, Medrano EE, Linskensi
973 M, Rubeljii I, Pereira-Smithii O, Peacocket M, Campisi J, Pardee B. 1995. A
974 biomarker that identifies senescent human cells in culture and in aging skin in vivo
975 (replicative senescence/tumor suppression/18-galactosidase) Communicated by
976 Arthur. *Cell Bioiogy* **92**:9363–9367.

977 Engler M, Fidan M, Nandi S, Cirstea IC. 2021. Senescence in RASopathies, a possible

novel contributor to a complex pathophenoype. *Mech Ageing Dev*. doi:10.1016/j.mad.2020.111411

Francis TG, Jaka O, Ellison-Hughes GM, Lazarus NR, Harridge SDR. 2022. Human primary skeletal muscle-derived myoblasts and fibroblasts reveal different senescent phenotypes. *JCSM Rapid Commun* **5**:226–238. doi:10.1002/RCO2.67

Franza BR, Maruyama K, Garrels JI, Ruley HE. 1986. In vitro establishment is not a sufficient prerequisite for transformation by activated ras oncogenes. *Cell* **44**:409–418. doi:10.1016/0092-8674(86)90462-9

Gilliam LAA, Moylan JS, Patterson EW, Smith JD, Wilson AS, Rabbani Z, Reid MB. 2012. Doxorubicin acts via mitochondrial ROS to stimulate catabolism in C2C12 myotubes. *Am J Physiol - Cell Physiol* **302**:195–202. doi:10.1152/AJPCELL.00217.2011/ASSET/IMAGES/LARGE/ZH001211679900 08.JPEG

Gilliam LAA, St. Clair DK. 2011. Chemotherapy-Induced Weakness and Fatigue in Skeletal Muscle: The Role of Oxidative Stress. *https://home.liebertpub.com/ars* **15**:2543–2563. doi:10.1089/ARS.2011.3965

Gutierrez L, Magee AI, Marshall CJ, Hancock JF. 1989. Post-translational processing of p21ras is two-step and involves carboxyl-methylation and carboxy-terminal proteolysis. *EMBO J* **8**:1093–1098. doi:10.1002/J.1460-2075.1989.TB03478.X

Hachet-Haas M, Converset N, Marchal O, Matthes H, Gioria S, Galzi J-L, Lecat S. 2006. FRET and colocalization analyzer—A method to validate measurements of sensitized emission FRET acquired by confocal microscopy and available as an ImageJ Plug-in. *Microsc Res Tech* **69**:941–956. doi:10.1002/jemt.20376

Hamsanathan S, Gurkar AU. 2022. Lipids as Regulators of Cellular Senescence. *Front Physiol* **13**:796850. doi:10.3389/FPHYS.2022.796850/BIBTEX

Harvey JJ. 1964. An Unidentified Virus which causes the Rapid Production of Tumours in Mice. Nat 1964 2044963 204:1104–1105. doi:10.1038/2041104b0

Hayflick L. 1965. The limited in vitro lifetime of human diploid cell strains. *Exp Cell Res* **37**:614–636. doi:10.1016/0014-4827(65)90211-9

Hiensch AE, Bolam KA, Mijwel S, Jeneson JAL, Huitema ADR, Kranenburg O, van

1008 der Wall E, Rundqvist H, Wengstrom Y, May AM. 2020. Doxorubicin-induced
1009 skeletal muscle atrophy: Elucidating the underlying molecular pathways. *Acta*
1010 *Physiol* **229**:e13400. doi:10.1111/APHA.13400

1011 Hu S., Liu B, Shang J, Lu T, Cai Y, Ding M, Zhou X, Wang X. 2023. PTGDS
1012 PROMOTES TUMORIGENESIS OF PERIPHERAL T CELL LYMPHOMA
1013 THROUGH REGULATING IRON METABOLISM. *Hematol Oncol* **41**:625–625.
1014 doi:10.1002/HON.3165_475

1015 Hu Shunfeng, Liu B, Shang J, Lu T, Ding M, Zhou X, Wang X. 2023. P1210:
1016 TARGETING PTGDS AS A NOVEL THERAPEUTIC APPROACH IN
1017 PERIPHERAL T CELL LYMPHOMA THROUGH REGULATING IRON
1018 METABOLISM. *HemaSphere* **7**:e6034196.
1019 doi:10.1097/01.HS9.0000971736.60341.96

1020 Hu S, Ren S, Cai Y, Liu J, Han Y, Zhao Y, Yang J, Zhou X, Wang X. 2021. Glycoprotein
1021 PTGDS promotes tumorigenesis of diffuse large B-cell lymphoma by MYH9-
1022 mediated regulation of Wnt–β-catenin–STAT3 signaling. *Cell Death Differ 2021*
1023 *293* **29**:642–656. doi:10.1038/s41418-021-00880-2

1024 Hu X, Zhang H. 2019. Doxorubicin-Induced Cancer Cell Senescence Shows a Time
1025 Delay Effect and Is Inhibited by Epithelial-Mesenchymal Transition (EMT). *Med*
1026 *Sci Monit* **25**:3617–3623. doi:10.12659/MSM.914295

1027 Hunter JG, Van Delft MF, Rachubinski RA, Capone JP. 2001. Peroxisome Proliferator-
1028 activated Receptor γ Ligands Differentially Modulate Muscle Cell Differentiation
1029 and MyoD Gene Expression via Peroxisome Proliferator-activated Receptor γ-
1030 dependent and -independent Pathways. *J Biol Chem* **276**:38297–38306.
1031 doi:10.1074/JBC.M103594200

1032 Irikura D, Aritake K, Nagata N, Maruyama T, Shimamoto S, Urade Y. 2009.
1033 Biochemical, Functional, and Pharmacological Characterization of AT-56, an
1034 Orally Active and Selective Inhibitor of Lipocalin-type Prostaglandin D Synthase.
1035 *J Biol Chem* **284**:7623–7630. doi:10.1074/JBC.M808593200

1036 Johnson-Arbor K, Dubey R. 2022. Doxorubicin. *xPharm Compr Pharmacol Ref* 1–5.
1037 doi:10.1016/B978-008055232-3.61650-2

1038 Jones KR, Elmore LW, Jackson-Cook C, Demasters G, Povirk LF, Holt SE, Gewirtz
1039 DA. 2005. p53-dependent accelerated senescence induced by ionizing radiation
1040 in breast tumour cells. *Int J Radiat Biol* **81**:445–458.
1041 doi:10.1080/09553000500168549

1042 Kirsten WH, Mayer LA. 1967. Morphologic Responses to a Murine Erythroblastosis
1043 Virus. *JNCI J Natl Cancer Inst* **39**:311–335. doi:10.1093/JNCI/39.2.311

1044 Konieczny SF, Drobes BL, Menke SL, Taparowsky EJ. 1989. Inhibition of myogenic
1045 differentiation by the H-ras oncogene is associated with the down regulation of
1046 the MyoD1 gene. *Oncogene* **4**:473–481.

1047 Krtolica A, Parrinello S, Lockett S, Desprez PY, Campisi J. 2001. Senescent
1048 fibroblasts promote epithelial cell growth and tumorigenesis: A link between
1049 cancer and aging. *Proc Natl Acad Sci U S A* **98**:12072–12077.
1050 doi:10.1073/pnas.211053698

1051 Land H, Parada LF, Weinberg RA. 1983. Tumorigenic conversion of primary embryo
1052 fibroblasts requires at least two cooperating oncogenes. *Nature* **304**:596–602.
1053 doi:10.1038/304596a0

1054 Lassar AB, Thayer MJ, Overell RW, Weintraub H. 1989. Transformation by activated
1055 ras or fos prevents myogenesis by inhibiting expression of MyoD1. *Cell* **58**:659–
1056 667. doi:10.1016/0092-8674(89)90101-3

1057 Lee BY, Han JA, Im JS, Morrone A, Johung K, Goodwin EC, Kleijer WJ, DiMaio D,
1058 Hwang ES. 2006. Senescence-associated β-galactosidase is lysosomal β-
1059 galactosidase. *Aging Cell* **5**:187–195. doi:10.1111/j.1474-9726.2006.00199.x

1060 Lee J, Choi KJ, Lim MJ, Hong F, Choi TG, Tak E, Lee S, Kim YJ, Chang SG, Cho JM,
1061 Ha J, Kim SS. 2010. Proto-oncogenic H-Ras, K-Ras, and N-Ras are involved in
1062 muscle differentiation via phosphatidylinositol 3-kinase. *Cell Res* **20**:919–934.
1063 doi:10.1038/cr.2010.92

1064 Li J, Guo C, Wu J. 2019. 15-Deoxy-Δ-12,14-Prostaglandin J2 (15d-PGJ2), an
1065 Endogenous Ligand of PPAR-γ: Function and Mechanism. *PPAR Res* **2019**.
1066 doi:10.1155/2019/7242030

1067 Livak KJ, Schmittgen TD. 2001. Analysis of Relative Gene Expression Data Using

Real-Time Quantitative PCR and the 2−ΔΔCT Method. Methods 25:402–408. doi:10.1006/METH.2001.1262

Lorentzen A, Kinkhabwala A, Rocks O, Vartak N, Bastiaens PIH. 2010. Regulation of Ras localization by acylation enables a mode of intracellular signal propagation. *Sci Signal* **3**. doi:10.1126/SCISIGNAL.20001370/SUPPL_FILE/3_RA68_SM.PDF

Lowe SW, Cepero E, Evan G. 2004. Intrinsic tumour suppression. *Nature* **432**:307–315. doi:10.1038/nature03098

Lu JY, Hofmann SL. 1995. Depalmitoylation of CAAX motif proteins. Protein structural determinants of palmitate turnover rate. *J Biol Chem* **270**:7251–7256. doi:10.1074/JBC.270.13.7251/ATTACHMENT/56A70B86-B9FE-4517-9BAB-74A5749981A0/TBL1

Luis Oliva J, Pé Rez-Sala D, Castrillo A, Martínez N, Cañ Ada ‡ FJ, Boscá L, Rojas JM. 2003. The cyclopentenone 15-deoxy-12,14-prostaglandin J 2 binds to and activates H-Ras.

Marcone S, Fitzgerald DJ. 2013. Proteomic identification of the candidate target proteins of 15-deoxy-delta12,14-prostaglandin J2. *Proteomics* **13**:2135–2139. doi:10.1002/pmic.201200289

Moiseeva V, Cisneros A, Sica V, Deryagin O, Lai Y, Jung S, Andrés E, An J, Segalés J, Ortet L, Lukesova V, Volpe G, Benguria A, Dopazo A, Aznar-Benitah S, Urano Y, del Sol A, Esteban MA, Ohkawa Y, Serrano AL, Perdiguero E, Muñoz-Cánoves P. 2022. Senescence atlas reveals an aged-like inflamed niche that blunts muscle regeneration. Nat 2022 6137942 613:169–178. doi:10.1038/s41586-022-05535-x

Morgenstern J, Fleming T, Kadiyska I, Brings S, Groener JB, Nawroth P, Hecker M, Brune M. 2018. Sensitive mass spectrometric assay for determination of 15-deoxy-Δ12,14-prostaglandin J2 and its application in human plasma samples of patients with diabetes. *Anal Bioanal Chem* **410**:521–528. doi:10.1007/s00216-017-0748-1

Noë S, Corvelyn M, Willems S, Costamagna D, Aerts JM, Van Campenhout A,

1098 Desloovere K. 2022. The Myotube Analyzer: how to assess myogenic features in
1099 muscle stem cells. *Skelet Muscle* **12**:1–12. doi:10.1186/S13395-022-00297-
1100 6/FIGURES/10

1101 Olson,' EN, Spizz G, Tainsky2 MA. 1987. The oncogenic forms of N-ras or H-ras
1102 prevent skeletal myoblast differentiation. *Mol Cell Biol* **7**:2104–2111.
1103 doi:10.1128/MCB.7.6.2104-2111.1987

1104 Parrinello S, Coppe JP, Krtolica A, Campisi J. 2005. Stromal-epithelial interactions in
1105 aging and cancer: Senescent fibroblasts alter epithelial cell differentiation. *J Cell*
1106 *Sci* **118**:485–496. doi:10.1242/jcs.01635

1107 Pylayeva-Gupta Y, Grabocka E, Bar-Sagi D. 2011. RAS oncogenes: weaving a
1108 tumorigenic web. *Nat Rev Cancer 2011 1111* **11**:761–774. doi:10.1038/nrc3106

1109 Robles SJ, Adami GR. 1998. Agents that cause DNA double strand breaks lead to
1110 p16(INK4a) enrichment and the premature senescence of normal fibroblasts.
1111 *Oncogene* **16**:1113–1123. doi:10.1038/sj.onc.1201862

1112 Rocks O, Peyker A, Kahms M, Verveer PJ, Koerner C, Lumbierres M, Kuhlmann J,
1113 Waldmann H, Wittinghofer A, Bastiaens PIH. 2005. An acylation cycle regulates
1114 localization and activity of palmitoylated ras isoforms. *Science (80-)* **307**:1746–
1115 1752. doi:10.1126/science.1105654

1116 Rommel C, Clarke BA, Zimmermann S, Nuñez L, Rossman R, Reid K, Moelling K,
1117 Yancopoulos GD, Glass DJ. 1999. Differentiation stage-specific inhibition of the
1118 Raf-MEK-ERK pathway by Akt. *Science (80-)* **286**:1738–1741.
1119 doi:10.1126/SCIENCE.286.5445.1738

1120 Santra T, Herrero A, Rodriguez J, von Kriegsheim A, Iglesias-Martinez LF, Schwarzl
1121 T, Higgins D, Aye TT, Heck AJR, Calvo F, Agudo-Ibáñez L, Crespo P, Matallanas
1122 D, Kolch W. 2019. An Integrated Global Analysis of Compartmentalized HRAS
1123 Signaling. *Cell Rep* **26**:3100-3115.e7. doi:10.1016/J.CELREP.2019.02.038

1124 Scholz ME, Meissner JD, Scheibe RJ, Umeda PK, Chang KC, Gros G, Kubis HP.
1125 2009. Different roles of H-ras for regulation of myosin heavy chain promoters in
1126 satellite cell-derived muscle cell culture during proliferation and differentiation. *Am*
1127 *J Physiol - Cell Physiol* **297**:1012–1018.

1128 doi:10.1152/AJPCELL.00567.2008/ASSET/IMAGES/LARGE/ZH001009605700
1129 06.JPEG

1130 Serrano M, Lin AW, McCurrach ME, Beach D, Lowe SW. 1997. Oncogenic ras
1131 provokes premature cell senescence associated with accumulation of p53 and
1132 p16(INK4a). *Cell*. doi:10.1016/S0092-8674(00)81902-9

1133 Shaner NC, Lin MZ, McKeown MR, Steinbach PA, Hazelwood KL, Davidson MW,
1134 Tsien RY. 2008. Improving the photostability of bright monomeric orange and red
1135 fluorescent proteins. *Nat Methods 2008 56* **5**:545–551. doi:10.1038/nmeth.1209

1136 Shelton DN, Chang E, Whittier PS, Choi D, Funk WD. 1999. Microarray analysis of
1137 replicative senescence. *Curr Biol* **9**:939–945. doi:10.1016/S0960-
1138 9822(99)80420-5

1139 Shibata T, Kondo M, Osawa T, Shibata N, Kobayashi M, Uchida K. 2002. 15-Deoxy-
1140 Δ12,14-prostaglandin J2. *J Biol Chem* **277**:10459–10466.
1141 doi:10.1074/jbc.m110314200

1142 Slanovc J, Mikulčić M, Jahn N, Wizsy NGT, Sattler W, Malle E, Hrzenjak A. 2024.
1143 Prostaglandin 15d-PGJ2 inhibits proliferation of lung adenocarcinoma cells by
1144 inducing ROS production and activation of apoptosis via sirtuin-1. *Biochim*
1145 *Biophys acta Mol basis Dis* **1870**. doi:10.1016/J.BBADIS.2023.166924

1146 Smuder AJ, Kavazis AN, Min K, Powers SK. 2011. Exercise protects against
1147 doxorubicin-induced oxidative stress and proteolysis in skeletal muscle. *J Appl*
1148 *Physiol* **110**:935–942.
1149 doi:10.1152/JAPPLPHYSIOL.00677.2010/ASSET/IMAGES/LARGE/ZDG004119
1150 5300006.JPEG

1151 Stein GH, Beeson M, Gordon L. 1990. Failure to phosphorylate the retinoblastoma
1152 gene product in senescent human fibroblasts. *Science (80-)* **249**:666–669.
1153 doi:10.1126/science.2166342

1154 Van Der Burgt I, Kupsky W, Stassou S, Nadroo A, Barroso C, Diem A, Kratz CP,
1155 Dvorsky R, Ahmadian MR, Zenker M. 2007. Myopathy caused by HRAS germline
1156 mutations: implications for disturbed myogenic differentiation in the presence of
1157 constitutive HRas activation. *J Med Genet* **44**:459–462.

doi:10.1136/JMG.2007.049270

Veliça P, Khanim FL, Bunce CM. 2010. Prostaglandin D2 inhibits C2C12 myogenesis. *Mol Cell Endocrinol* **319**:71–78. doi:10.1016/J.MCE.2010.01.023

Vetter IR, Wittinghofer A. 2001. The guanine nucleotide-binding switch in three dimensions. *Science (80-)* **294**:1299–1304. doi:10.1126/SCIENCE.1062023/ASSET/0AB072BE-F662-4796-8B33-AFF3C6AD829F/ASSETS/GRAPHIC/SE4419929006.JPEG

Wang X, Spandidos A, Wang H, Seed B. 2012. PrimerBank: A PCR primer database for quantitative gene expression analysis, 2012 update. Nucleic Acids Res 40. doi:10.1093/NAR/GKR1013

Wiley CD, Campisi J. 2021. The metabolic roots of senescence: mechanisms and opportunities for intervention. *Nat Metab 2021 310* **3**:1290–1301. doi:10.1038/s42255-021-00483-8

Wiley CD, Campisi J. 2016. From Ancient Pathways to Aging Cells - Connecting Metabolism and Cellular Senescence. *Cell Metab*. doi:10.1016/j.cmet.2016.05.010

Wiley CD, Sharma R, Davis SS, Lopez-Dominguez JA, Mitchell KP, Wiley S, Alimirah F, Kim DE, Payne T, Rosko A, Aimontche E, Deshpande SM, Neri F, Kuehnemann C, Demaria M, Ramanathan A, Campisi J. 2021. Oxylipin biosynthesis reinforces cellular senescence and allows detection of senolysis. *Cell Metab* **33**:1124-1136.e5. doi:10.1016/j.cmet.2021.03.008

Wiley CD, Velarde MC, Lecot P, Liu S, Sarnoski EA, Freund A, Shirakawa K, Lim HW, Davis SS, Ramanathan A, Gerencser AA, Verdin E, Campisi J. 2016. Mitochondrial dysfunction induces senescence with a distinct secretory phenotype. *Cell Metab* **23**:303–314. doi:10.1016/j.cmet.2015.11.011

Woods D, Parry D, Cherwinski H, Bosch E, Lees E, Mcmahon M. 1997. Raf-Induced Proliferation or Cell Cycle Arrest Is Determined by the Level of Raf Activity with Arrest Mediated by p21 Cip1. *Mol Cell Biol* **17**:5598–5611.

Yamamoto Y, Takase K, Kishino J, Fujita M, Okamura N, Sakaeda T, Fujimoto M, Yagami T. 2011. Proteomic Identification of Protein Targets for 15-Deoxy-Δ12,14-

1188 Prostaglandin J2 in Neuronal Plasma Membrane. *PLoS One* **6**:e17552.
1189 doi:10.1371/JOURNAL.PONE.0017552

1190 Yang G, Rosen DG, Zhang Z, Bast RC, Mills GB, Colacino JA, Mercado-Uribe I, Liu
1191 J. 2006. The chemokine growth-regulated oncogene 1 (Gro-1) links RAS signaling
1192 to the senescence of stromal fibroblasts and ovarian tumorigenesis. *Proc Natl*
1193 *Acad Sci U S A* **103**:16472–16477. doi:10.1073/pnas.0605752103

1194 Yen CC, Hsiao C Der, Chen WM, Wen YS, Lin YC, Chang TW, Yao FY, Hung SC,
1195 Wang JY, Chiu JH, Wang HW, Lin CH, Chen TH, Chen PCH, Liu CL, Tzeng CH,
1196 Fletcher JA. 2014. Cytotoxic effects of 15d-PGJ2 against osteosarcoma through
1197 ROS-mediated AKT and cell cycle inhibition. *Oncotarget* **5**:716.
1198 doi:10.18632/ONCOTARGET.1704

1199 Zindy F, Williams RT, Baudino TA, Rehg JE, Skapek SX, Cleveland JL, Roussel MF,
1200 Sherr CJ. 2003. Arf tumor suppressor promoter monitors latent oncogenic signals
1201 in vivo. *Proc Natl Acad Sci U S A* **100**:15930–15935.
1202 doi:10.1073/pnas.2536808100

1203 Zwerschke W, Mazurek S, Stöckl P, Hütter E, Eigenbrodt E, Jansen-Dürr P. 2003.
1204 Metabolic analysis of senescent human fibroblasts reveals a role for AMP in
1205 cellular senescence. *Biochem J* **376**:403–411. doi:10.1042/BJ20030816